COMPUTATIONAL EFFICIENCY OF A HYBRID MASS CONCENTRATION AND

SPHERICAL HARMONIC MODELING

by

Nathan Piepgrass

A thesis submitted in partial fulfillment
of the requirements for the degree

of

MASTER OF SCIENCE

in

Mechanical Engineering

Approved:

_____   _____
Dr. David Geller   Dr. Rees Fullmer
Major Professor   Committee Member

_____   _____
Dr. Jim Wheeler   Dr. Byron Burnham
Committee Member   Dean of Graduate Studies

UTAH STATE UNIVERSITY
Logan, Utah

2011

Abstract

Computational Efficiency of a Hybrid Mass Concentration and Spherical Harmonic Modeling

by

Nathan Piepgrass, Master of Science

Utah State University, 2011

Major Professor: Dr. David Geller
Department: Mechanical and Aerospace Engineering

Through Spherical Harmonics, one can describe complex gravitational fields. However as the order and degree of the spherical harmonics increases, the computation speed rises exponentially. In addition, for onboard applications of spherical harmonics, the processors are radiation hardened in order to mitigate negative effects of the space environment on electronics. But, those processors have outdated processing speeds, resulting in a slower onboard spherical harmonic program.

This thesis examines a partial solution to the slow computation speed of spherical harmonics programs. The partial solution was to supplant the gravity models in the flight software. The spherical harmonics gravity model can be replaced by a hybrid model, a mass concentrations model and a secondary (lesser degree or order) spherical harmonics model. That hybrid model can lead to greater processing speeds while maintaining the same level of accuracy.

To compute the mass values for the mass concentration model, a potential estimation scheme was selected. In that scheme, mass values were computed by minimizing the integral of the difference between the correct and the estimated potential.

The best hybrid model for the 8 degree and 8 order, 15 degree and 15 order, and 30 degree and 30 order lunar potential fields is developed following three different approaches: potential zeros method, gravitational anomalies method, and iterative method. Afterwards, the accuracy and computation time of the models are measured and compared to the primary spherical harmonic lunar model.

In the aftermath, while the best hybrid model for all three cases was able to run faster than the primary spherical harmonic model, it was unable to be sufficiently accurate to replace the primary spherical harmonic model. The mass estimation scheme is severely hindered by the

condition number and convergence issues resulting in inaccurate estimates for the mass values for a given distribution.

It is recommended to alleviate the condition number error by eliminating the inverse in the mass estimation scheme. Other recommendations include fixing the convergence error, investing in software and hardware development, and focusing on other hybrid research objectives.

(114 pages)

Contents

List of Tables

List of Figures

Chapter 1

Introduction

1.1 Processing Speed of Spherical Harmonics Software

Spherical Harmonics allows a potential to be mapped to a spherical coordinate geometry. Through empirical or analytical coefficients, Spherical Harmonics are able to describe potentials that are too difficult to solve using the fundamental potential field equations. Consequently, gravitational fields can be modeled using spherical harmonics [1].

Despite the ability of spherical harmonics to describe complex gravitational fields, the computation speed of spherical harmonics program increases as the degree and order increase (see Figure 1.1). A 100 degree and 100 order spherical harmonics requires about 2500% more computation time than 0 degree and 0 order model, the point mass gravity term μ/r^2.

The increase in computation time is a result of spherical harmonics being a finite series expansion that depend on coefficients, associated Legendre polynomials [2], and recursive relations [3]. As the order and degree of the spherical harmonic series increases, the number of coefficients and other variables grows exponentially. As a result, the spherical harmonic program is required to perform more calculations as the maximum degree and order increases.

To make matters worse, the higher degree and order spherical harmonics models are required to accurately model complex gravitational fields [4]. Those higher order and degree spherical harmonics models generate terms that become difficult to represent on a finite word length computer [5], resulting in more computationally expensive spherical harmonics gravitational software [6].

The computation time of the spherical harmonics has been a problem in the past. NASA and the aerospace community have implemented a Lunar spherical harmonic gravitational model in the flight computer of a lunar orbiter. When the spherical harmonic model was 8 degree and 8 order, the computation time of the model was satisfactory. However, when the spherical harmonics were set at 30 degree and 30 order to account for the complexity in the lunar gravitational field, the model required more computation time. Unfortunately, that additional time was deemed unsatisfactory.
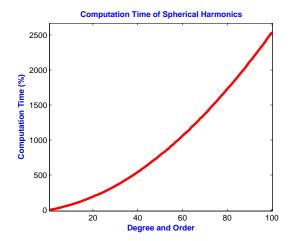
Figure 1.1: The additional computation time required for a Q degree Q order spherical harmonic model, where the values of Q are indicated in the x axis, in comparison to a 0 degree 0 order spherical harmonic model.

In another situation, the spherical harmonic computation time expense can hamper simulations. From previous research, computing a trajectory of a satellite using a 30 degree and 30 order spherical harmonic model can take about 250% longer than a 8 degree and 8 order model.

1.2 Radiation Hardened Effect on Onboard Spherical Harmonics Flight Software

For those cases where spherical harmonics gravitational software is used onboard the spacecraft, there are additional concerns.

The space environment can create errors, defects or other problems in the hardware or software. As a result, technological countermeasures are implemented to improve the resiliency of the hardware and software. However, those technological countermeasures decrease the overall quality of the computer resources.

As a result, the inferior computing resources, such as processing speed, will reduce the computation speed of the onboard spherical harmonics program. Hence, there is greater need to develop faster models to replace the spherical harmonics.

1.2.1 Space Environment Hazards and Effects on Electronics

The space environment consists of radiation belts, solar flares and cosmic rays which generate high to low energy particles with different compositions and varying fluxes [7].

As a result, there is potential for a spacecraft's software and hardware to be exposed to those

particles. If unprotected, that software and hardware could produce circuit failure [8], electrical spikes, burnout [9] and harmful discharges [10].

The space environment and its possible hazards have caused unexpected computer reboots [11], attitude control failure [10], and solar panel damage [7] in satellites and spacecraft. In 1992, a survey of 2500 satellite failures from 1962 to 1988 stated 21.4% of the failures were caused by space environment [12].

1.2.2 Radiation Hardened Electronics: Computational and Development Concerns

Since unprotected hardware and software have the capability to fail in the space environment, radiation hardened electronics was built using semiconductor processes, and manufactured with more transistors [13].

Currently, the radiation hardened processor RAD6000 unit, a radiation hardened microprocessor and RAM, are used for more than 150 spacecrafts, the earliest spacecraft was the Mars Pathfinder in 1996 [14].

The successor to RAD6000 was RAD750 [14]. Deep Impact launched in 2005 was one of the first spacecrafts to use the RAD750 computer unit. Since then, 30 additional spacecraft have used RAD750.

While the radiation hardened chips protects software and hardware from radiation, the radiation hardened electronics are power hungry, expensive [15] and slow (see Figure 1.2).

RAD6000 microprocessor performs at most between 20 to 33 MHz depending on the circuit board configuration. In contrast when the first RAD6000 unit was used in 1996, the best computer had 180 to 167 MHz more processing speed.

Even the most advanced processor, RAD750, has a maximum processing speed of 133 MHz [8] in comparison to 1.3 GHz processing speeds.

The computational performance of radiation hardened electronics is not sufficient to keep up with the newer technological advances. First, as the processing speed increases, the thermal dissipation and power requirements get larger. Second, as the electronics become smaller, the background radiation has a more severe effect [16].

While other researchers have looked at hardware and circuit architecture solutions, the radiation effects still remains problematic [8]. Even with improvements in radiation hardening, the
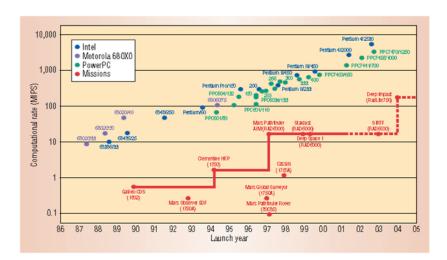
Figure 1.2: The computation rate (MIPS) is similar to processing speed. The red line refers to radiation hardened processors, while the green and blue dots represent commercial processors.

electronics are still behind their contemporary counterparts [17].

Chapter 2

Thesis Statement

2.1 Hypothesis

Spherical harmonics is an important tool for describing gravitational fields. However, the spherical harmonics require more computation time to describe more sophisticated gravitational fields. For onboard applications, the spherical harmonics program cannot utilize modern commercial processors when on satellites equipped with radiation hardened processors. As a result, the computation speeds of those onboard spherical harmonic programs become slower.

To solve this issue, previous researchers have looked at developing more efficient code [6], finding quicker recursive relations [5], and improving hardware and circuit architecture circuitry[17]. Despite those improvements, the processing speed of spherical harmonics remains problematic.

This thesis offers a partial solution.

The spherical harmonics can be replaced by a hybrid model, a mass concentrations model and a secondary (lesser degree or order) spherical harmonics model. The thesis is that the hybrid model can reduce required processing time while maintaining nearly the same level of accuracy.

The approach to the hybrid model can be seen in Figure 2.1. The primary or full spherical harmonic model can be broken up into individual expansion terms. The mass concentrations model will approximate several of those terms, while another spherical harmonic model will compute the rest.

2.2 Rationale

The justification can be seen by comparing the processing time of the mass concentrations model, and the spherical harmonics model in Figure 2.2. If properly optimized, the mass point concentration program can run faster than the optimal spherical harmonics program depending on the quantity of masses in the distribution, and the order and degree of the spherical harmonic model. That processing advantage allows the hybrid model to adjust the masses in the mass
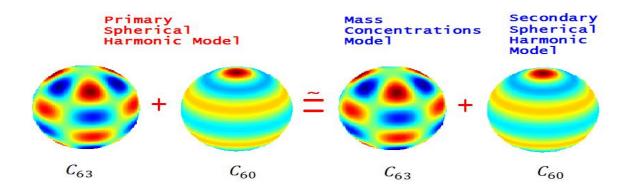
Figure 2.1: The original spherical harmonic model (on the left) approximately equivalent to the hybrid model (on the right) consisting of mass concentrations and a secondary spherical harmonic model.

concentration model, and the degree and order in the secondary spherical harmonic to achieve a faster computation speed than the primary spherical harmonic model.

As seen in Figure 2.2, the processing speed of the point mass version of the mass concentration model primarily depends on the number of point masses in a distribution. However, the spherical harmonics program's processing time only depends on the number of coefficients, a function of the order and degree. Hence, the processing speed of the hybrid model can be adjusted by altering the amount of masses and the coefficients.

In addition the spherical harmonics processing time increases as the degree and order increase, see Figure 1.1. As a result, there is a gap between the lowest spherical harmonic model and the N degree and M order models, which becomes longer as the N and M increases. If that gap is large enough, the mass concentration model could run within that time frame. Then the hybrid model could run faster than the primary spherical harmonic model.

For example, let the primary spherical harmonic model be a 15 degree and 15 order model. Let the secondary harmonic model be a 8 degree and 8 order model. The gap between the 15 degree and 15 order model to the 8 degree and 8 order model is about 4×10^{-5} seconds. Any mass concentration model with a computation time less than 4×10^{-5} seconds will assure that the hybrid model runs faster then the primary spherical harmonic model. To continue the example, let the mass concentration model have 20 masses, which would make the mass concentration model compute around 3×10^{-5} seconds. Thus, the hybrid model will run faster by 1×10^{-5} seconds, or 7%.
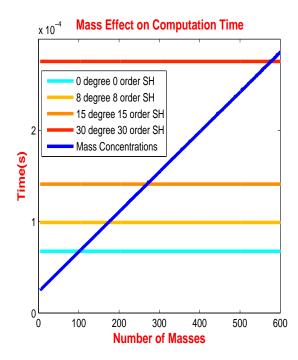
Figure 2.2: The processing time for the spherical harmonics and mass concentration models. The computation time for the spherical harmonics, and the mass concentration model were determined using Matlab's built in time measuring algorithms. The small variation in the computation time of mass concentration model is a result of background noise being unfiltered in previous algorithm.

2.3 Scope of Research

NASA and the aerospace community have explored various options to mitigate the poor processing speeds of the spherical harmonic model. In particular, one aerospace company wanted a solution to the poor performance of onboard 30 degree 30 order spherical harmonic models for orbiting lunar satellites. As a result, the scope of this research explores the validity of the hybrid model as a successful substitute for the onboard 30 degree and 30 order spherical harmonic model for satellites orbiting the moon. To allow examination of more configurations of hybrid models, the study is extended to 15 degree and 15 order, and 8 degree and 8 order. The scope of the research will be limited to the following parameters in Table 2.1.

As previously mentioned, the moon's gravitational field will be studied to address the problem faced by the aerospace community. In addition, the lunar gravitational field will be represented as spherical harmonic model from the most up to date coefficients which were determined empirically through Lunar Prospector and other lunar satellites. Those coefficients, referred as the LP75D, can be seen in the Appendix C.

The region of interest is the complete exterior gravitational field of the moon. The weight

Table 2.1: Scope of Research.

Maximum Harmonics		Potential Source			Other Parameters	
Primary Model		Planet	Type	Model	Region	Software
Degree	Order	Moon	Gravity	LP	Levie	Gottlieb
8	8					
15	15					
30	30					

matrix, W in the mass estimation scheme (see Equation 4.18) will be set to same parameters in reference [18].

To eliminate using unoptimized or slow spherical harmonic programs, the Gottlieb spherical harmonic software program will be implemented [6]. According to Gottlieb, the spherical harmonic software program offsets the singularities when taking the gradient of the potential in respect to the spherical coordinates [6]. In addition, Gottlieb uses the recursive relations that are numerically stable and accurate based on the research conducted by Lundberg [6].

Chapter 3

Literature Survey

3.1 Mass Concentrations and Estimation Schemes

From a historical perspective, the mass concentration models and estimation schemes were derived for lunar gravity missions. In 1968, Muller and Sjogren discovered mascons, short for mass concentrations, on the maria of the near side of the moon [8]. Another study found that using spherical harmonics to model those mascons may not be ideal. Thus, mass concentration models were proposed [19].

Mass concentration refers to collection of unconnected masses. For example, a mass concentration model can have point masses in grids across the Earth [20]. Each mass, though, has its own potential. So the overall potential from the various masses is

$$V = \sum_{i=1}^{n} m_i V_i \tag{3.1}$$

However, each author presents a different approach for determining the mass values, m_i. A few of those estimation techniques will be explained and critiqued.

In case of Ananda [21], orbital elements are extracted from the raw Doppler tracking data for Apollo 15, 16 satellites and Lunar Orbiter 5. Afterwards, a spline fit of the mean orbital elements are computed. At this point, the author differentiates the spline fit formula for orbital elements [22] and then calculates the average partials of the potential in respect to orbital elements [23]. In the aftermath, the result leads to values for each mass point.

Instead of orbital elements, L.Wong and other colleagues computed mass values by minimizing a quadratic sum of the observed residual Doppler vector, $\triangle C$, the Doppler variance matrix $\sum$, the initial state vector deviations $\triangle S$, and weighted by a priori state variance matrix $\sum_o$ [24].

$$Q = \triangle C^T \Sigma^{-1} \triangle C + \triangle S^T \Sigma_o^{-1} \triangle S \tag{3.2}$$

The previous mass estimation scheme has produced some appreciable results. For point masses, the mass concentration model can be easily adjusted to match the gravity field. In polar lunar orbits, the mass points did well [24].

However, there were some problems. Point masses are not realistic geometries for mascons, large circular gravitational anomalies [22]. In addition, there are singularity issues as the satellite or source gets close to the mass point [24].

While the previous mass estimation models relied on Doppler measurements, and orbital elements, Sterling Levie and other colleagues at Bellcom estimated the mass values by minimizing the integral of the difference between the true and the estimated potential over a volume in space [25].

$$f(v, \widetilde{v}) = \int_R (v - \widetilde{v})^2 d\tau \tag{3.3}$$

where $\widetilde{v}$ is the mass concentrations estimate of the potential, v is the spherical harmonic approximation of the true potential, and R is a volume in space.

After implementing least squares on the matrix version of the previous criteria, Equation 3.3 becomes

$$M = (J^T W J)^{-1} J^T W S \tag{3.4}$$

Where M is a vector of mass values. The S parameter is the set of expansion coefficients for the true potential, v. The coefficient matrix, J, has N columns of spherical harmonic coefficients for N masses. The coefficients can be translated from the origin [25], while describing spheroids, mass points and other shapes [26]. The weight matrix is defined as

$$W = \begin{bmatrix} A & 0 \\ 0 & A \end{bmatrix} \tag{3.5}$$

where A is the integral of pairs of associated Legendre polynomials over a given region.

The potential mass concentrations model was able to decently replicate the potential field represented by spherical harmonics for a given region of space [18]. However, there are some nuances which will be explained in the procedure section.

The strongest argument against using mass concentrations with spherical harmonics is the level of accuracy of the mass estimation scheme. After developing the mass estimation scheme,

Levie used it to compute the values for 21 mass points with the intention of replicating the lunar spherical harmonic potential field model within a restricted region of space. In the aftermath, the chosen mass distribution in the mass concentration model could not reproduce the effect of the coefficients in the lunar spherical harmonic model on the potential field [18]. As a result, the mass concentration model was unable to represent the lunar spherical harmonic model at all points within the selected region.

However, while not perfect, the mass concentrations model was satisfactory. It also did extremely well in fitting the L1 Lunar model in the interior region [18]. Levie also remarks that adding more mass points would increase the accuracy of the model. Another researcher, Chatfield, also states that given enough mass points, any spherical harmonic model can be replicated [20].

3.2 Hybrid Research and Development

After the initial research into mass points or disks, Wong, Ananda and other researchers claimed that a better model would be a composite of spherical harmonics and mass concentrations. Ananda wanted to combine the discrete point models and low order spherical harmonics [21, 23], but according to the abstracts reports on NASA technical reports server, Ananda didn't pursue the topic any further. On the other hand, Wong and his fellow colleagues attempted to combine the mass concentrations and spherical harmonics models.

There has been some previous research in combining mass concentration models and spherical harmonic models. In Wong's composite or hybrid model [24], a grid of mass points, with values estimated from Wong's scheme, were used for one region while the spherical harmonics were implemented for a different region.

The composite model, though, was flawed. First, the reliance on short increments of satellite data to compute errorless Doppler measurements didn't provide sufficient information to properly propagate the orbit. As a consequence, the results of the composite model, in comparison to more verifiable models, performed poorly in approximating the moon's prevalent gravitational forces [24].

Wong and his colleagues also concluded to wait for further and clearer information on the gravity of the far side of the moon before attempting further research.

Due to the quality and lack of satellite tracking data, additional efforts into combined lunar mass concentration and spherical modeling appeared to die out [19]. However, there is at least one

prevailing mass concentration and spherical harmonic hybrid model of the Earth.

A Mascon model [27, 28] uses time varying expansion coefficients, and blocks of masses to estimate mass variations on the surface of the earth. However, measuring the expansion coefficients has some complications. First, one needs access to a gravitational measuring device that is sensitive enough to measure mass variance in time. Second, in case of the GRACE satellites, there is aliasing and lack of sufficient information for submonthly stokes coefficients.

$$\triangle C_{nm}(t) = \frac{(1 + k'_n)R^2 \sigma(t)}{(2n + 1)M} \int Y^c_{nm}(\Omega)d\Omega \tag{3.6}$$

$$\triangle S_{nm}(t) = \frac{(1 + k'_n)R^2 \sigma(t)}{(2n + 1)M} \int Y^s_{nm}(\Omega)d\Omega \tag{3.7}$$

where n and m are the degree and order respectively, k'_n is the loading Love number, the ratio of additional potential produced by tides over the entire potential, of degree n, R is the mean radius and M is the mass of the Earth, Ω is a representation of surface area, $\sigma(t)$ is the mass of the layer over a unit of surface area at the epoch t and

$$Y^c_{nm} = P_{nm}(cos\theta)cos(m\phi) \tag{3.8}$$

$$Y^s_{nm} = P_{nm}(cos\theta)cos(m\phi) \tag{3.9}$$

are the Laplace spherical harmonic functions where the coordinates θ, and ϕ are respectively co-latitude, and longitude.

The previous mascon model was able to estimate mass variations on the surface of the earth, and oceanic currents [27].

Chapter 4

Theory

4.1 Spherical Harmonics

4.1.1 Description

Spherical Harmonics allows a potential to be mapped to a spherical coordinate geometry. Through empirical coefficients, spherical harmonics are able to describe potentials that are too difficult to solve using Newtonian or relativistic potential field equations. In general, the spherical harmonics can be derived from the Laplace equation [29] or from a spherical mass distribution [2].

For gravitational potentials, the spherical harmonics are

$$V(r, \theta, \phi) = -\frac{GM}{r} \sum_{n=0}^{\infty} (\frac{RE}{r})^n \sum_{m=0}^{n} P_{nm}(cos\theta) \left[C_{nm} cos(m\phi) + S_{nm} sin(m\phi) \right] \qquad (4.1)$$

where r is the radius,

θ is the colatitude,

ϕ is the longitude,

P_{nm} is the associated Legendre polynomial

RE is the equatorial radius of the potential source,

G is the gravitational constant

M is the mass of the potential source

and the stokes coefficients (C_{nm} and S_{nm}) are defined as

$$C_{nm} = (2 - \sigma_{om}) \frac{(n-m)!}{M(n+m)!} \iiint_M \left[\frac{r}{R} \right]^n D(r, \theta, \phi) cos\phi P_{nm} sin\phi cos(m\theta) r^2 dr d\theta d\phi \qquad (4.2)$$

$$S_{nm} = (2 - \sigma_{om}) \frac{(n-m)!}{M(n+m)!} \iiint_M \left[\frac{r}{R} \right]^n D(r, \theta, \phi) cos\phi P_{nm} sin\phi sin(m\theta) r^2 dr d\theta d\phi \qquad (4.3)$$

where D is the density of the potential source as a function of the spherical coordinates.

In the previous equations, the associated Legendre polynomial, P_{nm}, can be expressed in terms of the Legendre polynomial

$$P_{nm}(v) = (1 - v^2)^{m/2} \frac{d^m}{dv^m} P_n(v) \tag{4.4}$$

where the n indice is the degree and the m is the order [2].

4.1.2 Normalization

While the spherical harmonics can describe potentials, the large order and degree spherical harmonics models requires normalization of the coefficients and the associated Legendre polynomials. The normalization can also reduce the condition number of matrices made up of columns of spherical harmonic coefficients or associated Legendre polynomials.

In general, both the coefficients and the Legendre functions are fully normalized with a factor, N,

$$[C_{nm}]_N = \frac{C_{nm}}{N} \tag{4.5}$$

$$[S_{nm}]_N = \frac{S_{nm}}{N} \tag{4.6}$$

$$[P_{nm}]_N = P_{nm} N \tag{4.7}$$

where $[C_{nm}]_N$ and $[S_{nm}]_N$ are the normalized stokes coefficients,

$[P_{nm}]_N$ is the normalized associated Legendre polynomials,

and

$$N = \sqrt{\frac{(2 - \sigma_{m0})(2n - 1)(n - m)!}{(n + m)!}} \tag{4.8}$$

where m is the order

n is the degree,

σ_{m0} is a Kronecker delta function.

As the degree and order becomes larger, the N factor becomes significantly smaller. As a result, the unnormalized coefficients can become so large that it reaches the bit size of the

computer [5]. In the aftermath, for large degree and order models, the unormalized coefficients become truncated or set to zero, leading to significant errors.

While the spherical harmonic model is more accurate when using normalized coefficients and Legendre polynomials, the time to process that model becomes slower [6].

For matrices composed of coefficients, normalization of those coefficients leads to a better conditioned matrix. Normalization reduces the range of values between the minimum and maximum coefficient in the matrix. As a result, the range of eigenvalues of those matrices is smaller leading to a better condition number, a function of the eigenvalues of the matrix. However, minimizing the range of the values of the coefficients is not the only factor in reducing the condition number.

4.2 Mass Estimation Scheme

Of the mass estimation schemes explored, Levie's least squares scheme will be used. That scheme allows the hybrid model to successfully decouple the secondary spherical harmonic and mass concentration model.

Levie only considers a spherical harmonic and a mass concentration model. The secondary spherical harmonic model in the hybrid model is an adjustment to the least squares mass estimation scheme. The implementation of the hybrid model can be read in chapter 5.

The following section explains the derivation and application of Levie's mass estimation scheme.

4.2.1 Least Squares Mass Estimation

As mentioned in the literature survey, the least squares mass estimation scheme implements McLaughlin's Criterion [25].

$$f(v, \widetilde{v}) = \int (v - \widetilde{v})^2 d\tau \tag{4.9}$$

where v is the spherical harmonic model of the true potential

$$v = O^T S \tag{4.10}$$

where O contains a vector of Legendre polynomials multiplied by cosine or sine and the radial dilation,

$$O = \begin{bmatrix} \frac{1}{r} \\ \vdots \\ \frac{1}{r}\left(\frac{c}{r}\right)^n P_{nm}(cos\theta)cos(m\phi) \\ 0 \\ \vdots \\ \frac{1}{r}\left(\frac{c}{r}\right)^n P_{nm}(cos\theta)sin(m\phi) \end{bmatrix} \tag{4.11}$$

while S is a vector of Stokes coefficients multiplied by the mass of the potential source.

$$S = M_p \begin{bmatrix} C_{00} \\ C_{10} \\ \vdots \\ C_{nm} \\ S_{00} \\ S_{10} \\ \vdots \\ S_{nm} \end{bmatrix} \tag{4.12}$$

In Equation 4.9, the mass concentration potential, $\widetilde{v}$, is

$$\widetilde{v} = O^T JM \tag{4.13}$$

where M is a vector containing the mass values of the potential,

$$M = \begin{bmatrix} m_1 \\ m_2 \\ \vdots \\ m_q \end{bmatrix} \tag{4.14}$$

J is the coefficient matrix, and the indice q is the number of masses in the mass distribution.

$$
J = \begin{bmatrix}
C_{00_1} & C_{00_2} & \ldots & C_{00_q} \\
C_{10_1} & C_{10_2} & \ldots & C_{10_q} \\
\vdots & \vdots & \vdots & \vdots \\
C_{nm_1} & C_{nm_2} & \ldots & C_{nm_q} \\
S_{00_1} & S_{00_2} & \ldots & S_{00_q} \\
S_{10_1} & S_{10_2} & \ldots & S_{10_q} \\
\vdots & \vdots & \vdots & \vdots \\
S_{nn_1} & S_{nn_2} & \ldots & S_{nn_q}
\end{bmatrix}
\tag{4.15}
$$

In the mass distribution, every mass has its own spherical harmonic series and coefficients. Those coefficients become the columns in J, the coefficient matrix. If the mass is translated from the origin, its coefficients are translated accordingly [30].

Substituting Equations 4.13, and 4.10 into Equation 4.9 leads to

$$
\int (v - \tilde{v})^2 d\tau = (S - JM)^T W (S - JM)
\tag{4.16}
$$

where the weight matrix

$$
W = \int OO^T d\tau
\tag{4.17}
$$

is an integral of pairs of associated Legendre polynomials over a given region.

Differentiating Equation 4.16 in respect to M, and rearranging terms (see Appendix A), results in

$$
M = (J^T W J)^{-1} J^T W S
\tag{4.18}
$$

4.2.2 Mass Constraint

As the potential point gets farther away from the potential source, the point mass potential becomes more significant. In order to account for that effect, the estimated values for the mass concentration model must equal the total mass of the potential source.

The mass constraint is automatically held for good mass concentration models, when a mass is located at the center. In other cases, the mass constraint is enforced by modifying Equation 4.18.

First, the mass of the potential must equal the sum of the masses in a particular mass distribution,

$$M_p = \sum_{i=1}^{q} m_i \tag{4.19}$$

or in a matrix form as

$$M_p^2 = M^T \mathbf{1} M \tag{4.20}$$

where $\mathbf{1}$ is a matrix of ones.

In the Lagrange method,

$$f' = f + \lambda (M^T \mathbf{1} M - M_p^2) \tag{4.21}$$

where λ is a constant.

Like before, minimizing the previous equation leads to

$$M = (J^T W J + \lambda \mathbf{1})^{-1} J^T W S \tag{4.22}$$

Equation 4.22 can be solved by iteratively or analytically [25] determining the correct λ and M.

However, forcing the mass constraint through the use of Equation 4.22 has some disadvantages. If the condition number of $J^T W J + \lambda N$ is poor, some numerical solvers will become divergent. In addition, implementing the mass constraint can lead to different mass values than when the constraint is automatically satisfied.

4.2.3 Weight Matrix

In spherical harmonic representation, the weight matrix

$$W = \int O O^T d\tau \tag{4.23}$$

becomes

$$W = \begin{bmatrix} A & B \\ B^T & C \end{bmatrix} \tag{4.24}$$

where

$$A_{gh} = \int \int \int_R \frac{1}{r^2} \left(\frac{c}{r}\right)^{k+b} P_{km}(cos\theta)P_{bj}(cos\theta)cos(m\phi)cos(j\phi)r^2drd\phi d(cos\theta) \qquad (4.25)$$

$$B_{gh} = \int \int \int_R \frac{1}{r^2} \left(\frac{c}{r}\right)^{k+b} P_{km}(cos\theta)P_{bj}(cos\theta)cos(m\phi)sin(j\phi)r^2drd\phi d(cos\theta) \qquad (4.26)$$

$$C_{gh} = \int \int \int_R \frac{1}{r^2} \left(\frac{c}{r}\right)^{k+b} P_{km}(cos\theta)P_{bj}(cos\theta)sin(m\phi)sin(j\phi)r^2drd\phi d(cos\theta) \qquad (4.27)$$

The indices k, m, b and j follow the same triangular pattern, $00 \rightarrow 01 \rightarrow 10 \rightarrow 11 \rightarrow 20 \rightarrow 21...$, as the incides in the Stokes coefficients. If put into a n×d matrix, where n and d are integers, the Stokes coefficients are arranged as a lower triangle. The triangular pattern is defined as the indices of the Stokes coefficient located at some α row, and β column within the n×d matrix, where α and β both start at 1, and continue sweep along the triangular matrix until $\alpha = n$ and $\beta = d$. Note, that $\alpha \geq \beta$.

In the matrics A, B, and C, indice g indicates the row number and indice h represents the column number. Besides representing rows and columns, the indices g and h also indicates the set of digits in the triangular pattern. If the triangular pattern became a column vector, both g and h are the row indices. The sets of digits within that column vector become the values for k,m,b or j depending on the number for the indice g and h. For a given number g, the first digit is k and the second digit becomes m. Likewise, for a given h, the first digit becomes b and the second digit becomes j. For example, let g =1, then k=0 and m=0. Now, let h=2, then b=0 and j=1.

The integration region for A, B, and C are

$$\triangle_1 + c \leq r \leq \triangle_2 + c \qquad (4.28)$$

$$-a \leq cos\theta \leq a \qquad (4.29)$$

$$0 \leq \phi \leq 2\pi \tag{4.30}$$

where

c, Δ_1 and $\triangle_2$ are user specified radial constants,

a is the upper and lower bounds in the colatitude,

and ϕ is the range in longitude, preset at the full range.

However, since

$$\int_0^{2\pi} cos(m\phi)sin(j\phi)d\phi = 0$$

and

$$\int cos(m\phi)cos(j\phi)d\phi = \int sin(m\phi)sin(j\phi)d\phi \tag{4.31}$$

then C=A, and B=0. Hence, the weight matrix becomes

$$W = \begin{bmatrix} A & 0 \\ 0 & A \end{bmatrix} \tag{4.32}$$

An exact solution to the integration of the A matrix can be found in Levie's documentation [25]. Because the weight depends on region, degree and order, the weight matrix can be computed independently of the parameters that govern the mass distributions of the mass concentration model.

The weight matrix actually puts more emphasis on the coefficients to be matched in the mass value estimation scheme. Increasing the value of the diagonal elements in the weight matrix leads to more accurate estimations of those coefficients. However, at the same time, other coefficients can become less accurate. In other cases, for stable mass configurations, the changes in the diagonal elements will not change the accuracy of the coefficients.

4.2.4   Coefficient Matrix

Each mass in the configuration has its own coefficients, which become the columns of the coefficient matrix (see Equation 4.15). However, if a mass is relocated from the origin and the coordinate system does no move with the mass, then the coefficients of that mass require a translation

transformation [30]. To see how the Stokes coefficients transform for spheroids, see appendix.

For point masses, when a mass is translated from the origin, but remains within the space occupied by the potential source, the new coefficients are

$$
\begin{bmatrix} C'_{km} \\ S'_{km} \end{bmatrix} = \sum_{L=0}^{k} \left(\frac{r'}{RE}\right)^{k-L} \frac{k!}{L!(k-L)!} C_{L0}(2 - \sigma_{m0}) \frac{(k-m)!}{(k+m)!} P_{km}(cos\theta) \begin{bmatrix} cos(m\phi) \\ sin(m\phi) \end{bmatrix} \tag{4.33}
$$

where r' is the translated distance, θ is the colatitude, ϕ is the longitude, P_{nm} is the associated Legendre polynomial, C_{LO} is the mass' old C coefficient of degree L and 0 order, C'_{km} and S'_{km} are the new translated coefficients, and RE is the equatorial radius of the matching potential. A proof of Equation 4.33 is also provided in the Appendix B.

One important outcome from translating the spherical harmonics is that the new coefficients are linear combinations of all the previous ones. The C_{00} remains unmodified despite the location, size or shape of the mass.

After the mass values are known, the mass concentration model can be converted back into a spherical harmonic model. To do so, the coefficients for the equivalent spherical harmonic model are generated as

$$
\widetilde{S} = JM \tag{4.34}
$$

4.2.5 Accuracy Limitations of Mass Estimation Scheme

If the coefficient matrix is full rank, then the mass values can be computed as

$$
M = J^{-1}S \tag{4.35}
$$

As long as the coefficient matrix, J, is full rank, the computed mass values have no error.

Since the coefficient matrix depends on the mass distribution, a correct mass distribution requires satisfying the conditions for the coefficient matrix to be full rank. However, in this case, the coefficient matrix is composed of spherical harmonic coefficients, resulting in some rows of the coefficient matrix being zero. As a result, the coefficient matrix can never be a full rank matrix. As a consquence, the mass estimation scheme cannot determine values for masses in the mass distribution that will exactly replicate the spherical harmonic model.

4.2.6 Condition Number Errors

Poorly conditioned coefficient and weight matrices produce errors in estimating the mass values. In mass estimation scheme, Equation 4.18, there is an inverse of the coefficient matrix times the weight matrix, $\left[J^T W J\right]^{-1}$. If those matrices are poorly conditioned, then the inverse will produce some error depending on the condition number of the matrices. In addition, the lack of a proper inverse can also lead to numerical solver aborting before converging to the correct lambda in the mass constraint formulation, Equation 4.22.

Figure 4.1 shows the average error that occurs when taking an inverse of a poorly conditioned matrix on a log-log scale. For perfect conditioned matrix, P,

$$P^{-1}P = \mathbf{1} \tag{4.36}$$

where $\mathbf{1}$ is the identity matrix. If the matrix Q was poorly conditioned, then

$$Q^{-1}Q = \mathbf{1} + e \tag{4.37}$$

where e is some error.

The percent error in Figure 4.1 is the percent difference between the average of the diagonal elements of the perfect condition matrix and the poorly conditioned matrix, Equations 4.36, and 4.37. In the aftermath, the error from the condition number increases exponentially.

Poorly conditioned coefficient and weight matrices can be improved by normalizing the coefficients and Legendre polynomials,

$$J = J/N \tag{4.38}$$

$$W = WN^2 \tag{4.39}$$

where N is the normalization factor (see Equation 4.8). This normalization routine does not interfere with the final result, for substituting the previous equations leads to

$$M = (\frac{J^T}{N}WN^2\frac{J}{N})^{-1}\frac{J^T}{N}WN^2\frac{S}{N} \tag{4.40}$$

Cancelling out terms results in the same equation for the estimating the mass values
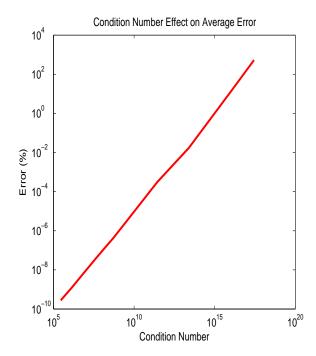
Figure 4.1: The Estimated Condition Number Error

$$M = (J^T W J)^{-1} J^T W S \tag{4.41}$$

With the normalization factor in place, the condition of the matrices is vastly reduced, for the condition number is defined as the ratio of the largest to smallest singular value of the matrix, which depend on the range of values, size of matrix and other factors. Normalization reduces the range of values within the matrix, but is not the only factor.

Besides normalizing the matrices, increasing the linear independence of the matrix also tends to lower the condition number of the matrix. For the coefficient matrix, increasing the linear independence of the matrix requires the masses to be located as far from each other as possible. In addition, the number of masses must not exceed the rank of the coefficient matrix.

Decreasing the size of the matrices also improves the condition number. The weight matrix in particular benefits as result of reducing the range of values between the integrals of pairs of Legendre polynomials.

4.2.7   Convergence

When computing the gravitational acceleration, G_a, the mass concentration model uses the point mass gravity equation,

$$G_a = G \sum_{i=1}^{Q} m_i \frac{\overline{r_i}}{\|\overline{r_i}\|^3} \tag{4.42}$$

where G is the gravitational parameter, m_i and r_i are respectively the mass value, and position associated with the ith mass. Q is the number of masses in a mass distribution.

However, the mass estimation scheme uses spherical harmonics as the gravitational expression for the individual masses. So up to some order and degree, each mass is represented by some finite limit of terms in Equation 4.1. Since the terms are finite, the estimated mass values do not take into account the error between the spherical harmonic series truncated at some order and degree, and the exact mass point Equation 4.42.

As a result, for each computed mass value, there is some error as a result of the spherical harmonic series not converging sufficiently to the exact point mass gravity equation. As seen in Figure 4.2, the spherical harmonic representation converges to the mass point Equation 4.42 as the degree and order of the maximum coefficient in the coefficient matrix increases.

While the convergence error for a mass configuration depends on the degree and order, it also is influenced by location of those masses from the center of the potential source. The latter is primarily due to the coefficients becoming smaller in value as the evaluation point moves away from the surface of the potential source.

So, decreasing the error between the exact point mass gravity model and the equivalent spherical harmonic model requires increasing the maximum degree and order of the coefficients in the coefficient matrix.
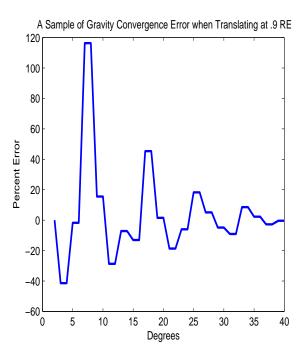
Figure 4.2: The convergence rate of a mass located away from the origin. The x axis shows the maximum degree of the coefficients for each of the masses. The y axis displays the percent error in gravitational acceleration at a point close to the surface between the exact equation (see Equation 4.42) and the equivalent spherical harmonic model (see Equations 4.34 and 4.1).

Chapter 5

Procedures

5.1 Hybrid Modeling Restrictions

Of the possible mass estimation schemes, Levie's least squares scheme will be used. That scheme allows the hybrid model to successfully decouple the secondary spherical harmonic and mass concentration model. However, the potential estimation scheme has some restrictions.

There can be significant numerical error if the condition number of the factor $J^T W J$ is poor. To alleviate the problem requires avoiding over constrained mass distributions and in some cases unnormalized coefficient and weight matrices. Even with a decent condition number and appropriate potential, it is possible for the mass configuration to have a center of mass displaced from the origin. Since that misalignment can be problematic, there is additional weight to match coefficients C_{10} and C_{11}.

5.2 Hybrid Modeling Approaches

Due to lack of uniqueness for a mass distribution, mass estimation scheme, and spherical harmonic representation, there isn't a best approach for constructing a hybrid model. However, there are approaches that are better than others, which are as follows.

5.2.1 Potential Zeros

The first method is called potential zeros approach. It follows Levie's research method [18], in which Levie consulted the multipoles of the potential to determine the placement of the masses. According to Levie, the multipoles is an arrangement of masses whose placement is located where zeros of potential occur.

With spherical harmonics representing the potential,

$$V(r,\theta,\phi) = -\frac{GM}{r} \sum_{n=0}^{\infty} (\frac{RE}{r})^n \sum_{m=0}^{n} P_{nm}(cos\theta) \left[C_{nm}cos(m\phi) + S_{nm}sin(m\phi) \right] \qquad (5.1)$$

a zero of a potential occurs in latitude when the associated Legendre polynomials, $P_{nm}(cos\theta)$ becomes zero. In practice, computing the zeros of associated Legendre polynomials can be complicated. For each associated Legendre polynomial is a function that changes form depending on the order and degree. In addition, those functions are mostly nonlinear in trigonometric functions of latitude, θ. So instead of numerical solving or estimating those zeros, Levie just places zeros uniformly in latitude depending on the amount of masses desired for the distribution.

Another zero of the potential occurs if one of the Stokes coefficients is zero. If all the C_{nm} coefficients are zero, then a zero of the potential exists at an interval of

$$\phi = 90 : \frac{90^0}{m} : 360 \tag{5.2}$$

On the otherhand, if the S_{nm} coefficients are all zero, then

$$\phi = 0 : \frac{180^0}{m} : 360 \tag{5.3}$$

Out of the two previous equations, in accordance with Levie's potential zeros approach, only Equation 5.3 will be used in the potential zeros approach. As a result, the approach will be aligned with Levie's research method.

The zeros of the potential form planes or circles on the surface of the potential (see Figure 5.1). A zero in latitude is a horizontal circle, while a zero in longitude is a vertical circle. After locating the zeros or circles, a mass is placed at the intersection of the vertical and horizontal circles.

In addition to those masses located at the zeros of the potential, another mass was placed at the center of the potential in order to replicate the mass point gravity term and to account for the spherical matter distribution of the potential body.

Theoretically, all the masses in the distribution were initially together at the center. The reason for doing so was to agree with a concept of multipoles theory of having negative and positive masses cancel each other leaving only their potential contributions behind. But due to numerical instabilities, the masses were expanded radially until some appropriate compromise between numerical stability and compliance to the theory of multipoles.

When applying this approach to the hybrid model, the secondary spherical harmonic model
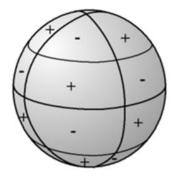
Figure 5.1: The circles on the sphere represents the zeros of the potential. The horizontal circles are zeros of the associated Legendre polynomials. The other circles are due to zeros of the sine or cosine functions in the potential. The negative and positive signs reflect the magnitude of the potential within the region bounded by the neighboring circles.

only contains the S coefficients, while the C coefficients are set to zero. The mass concentration model, likewise, takes all the C coefficients and some of the S coefficients depending on the degree, order and hybrid configuration.

Conditioned Matrices

For higher order models, the symmetric configuration of the mass distribution will lead to greater condition numbers. The symmetry of the mass distribution generates similar columns in the coefficient matrix resulting in inaccurate inverse of $J^T W J$.

To decrease the condition number of the coefficient matrix, the mass distribution was conditioned. After the potential zeros approach generates the mass distribution, row reduced echelon form of the coefficient matrix for that mass distribution is computed. The columns of the row reduced echelon form that are not composed of zeros and a one indicate a mass that is not independently placed or too similar to other masses in the mass distribution. The locations of those dependent masses are then adjusted in latitude by one degree resulting in a new mass distribution.

The previous procedure was repeated three times for the given mass distribution. It should be noted that for very poor locations of the masses in the mass distribution, more iterations are required. In addition, the final radial position of the masses varied due to the conditioning of the coefficient matrix and the initial mass distribution.

5.2.2 Gravitational Anomalies

While the potential zeros approach consults the potential, the gravitational anomalies method examines the gravity from a potential body. In practical terms, the gravitational anomalies, places where the gravity is not uniform, has been a tool in determining the mass locations for other mass concentration researchers [23, 24]. In addition, Levie also claims that using inhomogeneous regions to place masses is reasonable. Hence, this procedure is implemented in this thesis.

The first step in the gravitational anomalies approach is to generate a gravitational map displaying the gravitational anomalies of the potential body. The gravitational map for this approach is generated by setting the grid points every 1 degree in longitude and latitude and at zero altitude. Next, at each grid point, the gravitational acceleration variation is computed using a spherical harmonic gravity program, and is calculated as

$$a = \sqrt{a_{total} - a_j} \tag{5.4}$$

where a_{total} is the total gravitational acceleration some order m and degree n, a_j is the gravitational acceleration with order m=0, and degree n, where m and n are the maximum order and degree respectively [4].

The height of the evaluation surface, the set of altitudes where the gravitational acceleration are computed, can alter the shape and quantity of the gravitational anomalies. As the evaluation surface increases in altitude, the weaker gravitational anomalies will diminish and won't be displayed on the gravitational map. On the other hand, if the surface map is generated inside the gravitational body itself, the Stokes coefficients will lose validity. Hence, the best location of the evaluation surface occurs at the surface of the potential body. For the moon, evaluation surface was approximated as a spherical shell.

After the map is generated, a mass point is placed at the estimated center of each gravitational anomaly. Like the potential zeros approach, a mass is also positioned at the center of the potential source. By placing a mass at the center, the mass concentration estimation scheme is able to satisfy the mass constraint without using Equation 4.22. This is beneficial since if the condition number of the coefficient and weight matrices is too high, some numerical solvers will not be able to determine λ in Equation 4.22.

When the configuration of the hybrid model is chosen, the secondary spherical harmonic

model takes only the oblatness coefficients, the J coefficients or when m=0. The values for the rest of coefficients become zeros. The mass concentration model is assigned every coefficient of the primary spherical harmonic model. Those coefficients used by the secondary spherical harmonic model become equal to zero in mass concentration model.

5.2.3   Iterative Approach

The iterative approach implements Matlab 2010 built in *fmincon* function, which iteratively minimizes a function with some constraints. The *fmincon* program itself is well documented and very robust. It is capable of not mistaking a local maximum as a minimum to the function. In this case, that function is the average gravitational acceleration error between the hybrid and primary spherical harmonic models for a set of grid points.

While all those grid points were set at zero altitude, the placement in longitude and latitude varied depending on the degree and order of the primary spherical harmonic model. For spherical harmonic models lower or equal to 15 degree 15 order, the grid points were set at 5 degrees in longitude and latitude. Likewise, since the computation time to compute the gravitational maps become significant for higher degree and order models, the grid points were to set at 10 degrees in longitude and latitude for spherical harmonics higher than 15 degree 15 order.

Besides the grid points, the initial mass distribution for the iterative approach was configured to reduce the condition number of $J^T W J$ in the mass estimation scheme, Equation 4.18. For a given mass quantity, the masses were distributed symmetrically in latitude and longitude. Depending if the counter for each mass was odd or even, the radial position of the mass would be B×RE or (B+1)×RE, where B is a value such that for a given degree and order the error in the mass estimation from the condition number and convergence would be minimized, see Table 5.1. That B value can be determined by examining the plots for condition number and convergence errors.

Out of the four optimization algorithms available in *fmincon* , the active set algorithm will be used since, for this case, it generates results similar to other algorithms. However, the active set algorithm does use larger steps sizes, and does not take as many iterative steps in comparison to the interior point algorithm. However, the active set algorithm is faster than the other three algorithms.

Table 5.1: Shows the B values for the different degree and order models. The B value determines the radial locations of the masses in the initial mass distribution.

Model	B
8 degree 8 order	.3
15 degree 15 order	.5
30 degree 30 order	.7

The primary disadvantage in the *fmincon* function is that it is computationally expensive. The computation time of the fmincon program increases quadratically as more parameters are introduced. As a result, the higher order models with their more massive mass distributions take much longer to process.

Optimization Theory

To understand more about the active set algorithms, the following summarizes the general process of the active set algorithm.

The active set algorithm implements a sequential quadratic programming optimization scheme to solve the Karush-Kuhn-Tucker equations, several equations relating the constraints and minimized functions. First, the algorithm solves a quadratic programming subproblem by linearizing the constraints and solving for various variables. Afterwards, the Hessian of the Lagrangian is updated at each iteration using the Broyden-Fletcher-Goldfarb-Shanno (BFGS) formulation which approximates Newton's method for nonlinear optimization. The process is iterated until the derivative of the function is under some specified tolerance, and the constraints are satisfied.

5.3   Hybrid Configurations

Besides the three different approaches to determine a mass distribution, there are also at least two ways to configure the different hybrid models. In this paper, those categories are called lower, and upper hybrid models.

5.3.1   Lower Hybrid Configuration

Initially, the mass concentration model is assigned to match all the coefficients of the primary spherical harmonic model. So, the S vector of the mass estimation scheme

$$M = (J^T W J)^{-1} J^T W S \tag{5.5}$$

has all the coefficients of the primary spherical harmonic model. The weight and coefficient matrices are determined using the iterative, potential zeros or gravitational anomalies approach.

For example lets start with the secondary spherical harmonic model, the spherical harmonic model in the hybrid model, at 0 degree 0 order, which is just the point mass gravity term. However, modeling that mass point gravity term is already taken into account by the mass concentration model. As a result, the secondary spherical harmonic model does not compute the mass point gravity term. The previous hybrid configuration can be defined as a Y degree M order mass concentration model and a 0 degree 0 order secondary spherical harmonic model for a Y degree M order primary spherical harmonic model where Y and M are integers.

Now, if the secondary spherical harmonic model is at τ degree and ψ order, the Stokes coefficients of the secondary spherical harmonic model are same Stokes coefficients, up to τ degree and ψ order, of the primary spherical harmonic model. At the same time, those coefficients assigned to the secondary spherical harmonic model become zeros in the S vector. For example, let the primary spherical harmonic model be 8 degree 8 order. Then the S vector in the mass estimation scheme for the mass concentration model is assigned all the coefficients up to 8 degree 8 order. Now, let the secondary spherical harmonic be 8 degree 0 order. Then that secondary spherical harmonic model has all coefficients from 1 degree 0 order to 8 degree 0 order from the primary spherical harmonic model. In the mass concentration model, all the coefficients in the S vector from 1 degree 0 order to 8 degree 0 order become equal to zero. The rest of the coefficients, from 8 degree 0 order to 8 degree 8 order remain unchanged. Note, since the mass concentration model is estimating the point mass gravity term, the 0 degree 0 order coefficient is still equal to 1.

While the secondary spherical harmonic model increases in degree and order, the mass distribution of the mass concentration remains fixed. That mass distribution for this research was generated when the hybrid configuration was Y degree M order mass concentration model, 0 degree 0 order secondary spherical harmonic model, where Y is the degree and M is the order of the primary spherical harmonic model.

Since the secondary spherical harmonic model can have a smaller degree and order than the primary spherical harmonic model, the secondary spherical harmonic model runs faster than the primary spherical harmonic model. If the difference in computation speeds of those models is large enough, the mass concentration model can be computed within the time frame between the

two computation speeds. As a result, the hybrid model can have a faster computation speed than the primary spherical harmonic model.

However, the disadvantage in using this configuration is the lack of accuracy. The mass estimation scheme can not generate mass values that will exactly replicate the assigned the coefficients from the primary spherical harmonic model. As a result, more coefficients assigned to the mass concentration model will result in more error.

Despite its inaccuracy, the lower hybrid configuration is used in this research paper. As will be seen, the lower hybrid configuration is the only configuration capable of generating a hybrid configuration with a faster processing speed than the primary spherical harmonics model.

5.3.2   Upper Hybrid Configuration

The upper hybrid configuration is the exact opposite of the lower hybrid configurations. Initially, the secondary spherical harmonic model is assigned all the coefficients from the primary spherical harmonic model. The mass concentration model at this point does not have any coefficients, except for the point mass term.

So, the first upper hybrid configuration is defined as a 0 degree 0 order mass concentration model, Y degree M order secondary spherical harmonic model, and N degree M order primary spherical harmonic model, where Y and M are integers.

Now, if the S vector in the mass estimation scheme has a maximum degree Ω and a maximum order ξ, the S vector is composed of the Stokes Coefficients, up to Ω degree and ξ order, from the primary spherical harmonic model. For example, if the primary spherical harmonic model was 8 degree 8 order, the S vector has all coefficients of the primary spherical harmonic model up to 8 degree 8 order.

At the same time, those coefficients assigned to the mass concentration model become zeros in the secondary spherical harmonic model. Continuing the previous example, the Stokes ceofficients, from 0 degree 0 order to 8 degree 2 order, in secondary spherical harmonic model are equal to zero . Likewise, the Stokes ceofficients of the secondary spherical harmonic model from 8 degree 2 order to 8 degree 8 order are equal to the same Stokes coefficients of the primary spherical harmonic model.

Unlike the lower hybrid configuration, the mass distribution is not necessarily fixed. For every increase in degree and order, a new mass distribution must be computed.

Out of the hybrid models that are categorized as upper hybrid configurations or lower hybrid configurations, the hybrid models grouped as upper hybrid configurations are more accurate in replicating the primary spherical harmonic model. That is due to the upper hybrid configuration assigning fewer coefficients to the mass concentration model, the primary source of the error in the hybrid model.

However, since the secondary spherical harmonic model has the same degree and order of the primary spherical harmonic model, the processing speed of the primary and secondary spherical harmonic model will always be equal. Hence, any implementation of the mass concentration model will result in a hybrid model with a slower processing speed than the primary spherical harmonic model.

5.4   Other Mass Distribution Settings

The three different approaches describe how to find a mass distribution. However, there are additional parameters that need to be determined: region and adjustments of the weight matrix, normalization of coefficients and mass quantity limit.

5.4.1   Weight Matrix Region

The weight matrix requires a region of space to be specified before the integrals of the Legendre polynomials can be computed. That region affects how the weight matrix places emphasis on specific coefficients. Since there is no particular region of interest, the region was set to Levie's specifications in reference [25], a finite sphere around the moon.

5.4.2   Important Weighted Coefficients

Among the coefficients of the potential, the most important ones to match are C_{00}, C_{10}, C_{11}, S_{11}, S_{21}, and C_{21} [31]. The following gives a brief description.

C_{00} is the point mass coefficient, the largest gravitational term in the spherical harmonics expansion. If the mass constraint is automatically met, then the mass concentration model is able to match C_{00} extremely well.

Having C_{10}, C_{11}, and S_{11} set to zero assures that the mass distribution has its origin located at the center of coordinate system. If those coefficients are not matched entirely, then the there will be some misalignment errors in the gravitational acceleration from the mass concentration model.

S_{21} and C_{21} describe the main inertia axis of the planet. Any error would result in the mass concentration model rotation axis not aligned with the planet's inertia axis.

Due to the arrangement of the coefficient matrix, the S_{21} and S_{11} are matched perfectly by the mass concentration model. So, C_{10}, C_{11}, and C_{21} are the remaining coefficients that need to be matched in order to avoid misalignment errors.

To do so, diagonal elements in the weight matrix that correspond to those coefficients were amplified by 2×10^4. That value was selected by minimizing the condition number of the weight matrix while seeing a significant weight in the estimates of the desired coefficients.

5.4.3   Normalization Routine

As discussed in this paper, normalization helps to improve the condition number of the coefficient and weight matrices. Out of several normalization schemes, the spherical harmonics model will be fully normalized as seen in Equation 4.8.

5.4.4   Mass Quantity Limit

When it comes to matching a potential, the accuracy and the processing speed of the mass concentration model depends on the number of masses in the distribution. As the number of masses increase, the accuracy improves until there are more masses than coefficients. On the otherhand, increasing the masses also decreases the overall processing speed of the hybrid model.

The quantity of masses in the mass distribution are provided in Table 5.2. For a given N degree and M order, where N and M are integers, the computation time of the primary spherical harmonics was determined. Afterwards, the computation time of a hybrid model with the secondary spherical harmonic model of N degree 0 order and a mass concentration model with a variable number of masses was computed. The degree and order of the primary spherical harmonic model are tabulated in the first two columns on the left. The processing gain of 5, 10, and 20 is the percent difference between the computation speeds of the primary spherical harmonic model and the hybrid model. The number of masses in the mass concentration model that allows the hybrid model to have a particular processing gain with the primary spherical harmonic model of a given

Table 5.2: Number of masses in the mass concentration model required to achieve a 5, 10, or 20% computation speed in comparison to the primary spherical harmonic model.

Number of Masses Required to Achieve Processing Gain in the Hybrid Model				
Model		Processing Gain (%)		
Degree	Order	5	10	20
8	8	61	32	N/A
15	15	296	253	167
30	30	1022	941	774

degree and order is shown in the 3 by 3 white colored matrix. At certain mass quantities, the hybrid model can have a faster processing speed than the primary spherical harmonic model.

The table provides a reference to set the processing gains of the hybrid models by constraining the number of masses in the mass concentration model to a specified limit. In addition, using those masses requires the coefficients of the secondary spherical harmonic model to be restricted to the oblateness coefficients, C_{n0}.

5.4.5 Selection of a Hybrid Configuration

The lower hybrid configuration will be used in order to enhance the processing capabilities of the hybrid model. Thus, the mass concentration model will be assigned all coefficients of the primary spherical harmonic model. Any coefficients assigned to secondary spherical harmonic model are set to equal zero in the mass concentration model.

5.4.6 Center of Mass Constraint for Mass Distribution

As described in the three different approaches, a mass is located in the center of the potential body. As a result, for good mass distributions, the C_{00} term in the primary spherical harmonic model will be very well estimated by the mass distribution. Hence, for all models, the secondary spherical harmonics has $C_{00} = 0$.

5.5 Metrics

If the hybrid model is a capable substitute for the primary spherical harmonic model, it needs to accomplish two things: accuracy and speed. To determine if the hybrid model achieves those two metrics requires elaboration on how the metrics are measured, and other important and

relevant information.

5.5.1 Computation Speed

Measurement

The spherical harmonic program is tested for computation time by examining the amount of time to process the potential and gravity vectors for a given position.

The mass concentration has its own program where gravity and potential vectors are computed for a position. Like the spherical harmonics, the computation time of mass concentration model will be measured in the same manner.

The mass concentration model relies on an optimized point mass gravity program. The primary and secondary spherical harmonics models implement Gottlieb's algorithm [6]. However, the processing speed of mass concentration, primary and secondary spherical harmonics models are measured using Matlab's built in *tic toc* function. Since that function is susceptible to noise from other programs running in the background, the processing time for each hybrid and primary spherical harmonic model was averaged over 4000 runs.

Processing Speed Performance

The processing speed of the processor in the computer is not the only factor in determining the computation speed of the computer. The processor's performance is generally dependent on two factors: clock speed and architecture. The clock speed is a measurement of the overall processing speed in performing tasks. The architecture measures how efficient the processor is working on those tasks. Consequently, it is possible for two processors to have the same speed, but not the same efficiency. So, the computation time spent to complete a task is a combination of the processor's clock speed and architecture.

Increasing the processing speed and efficiency, though, may not help in improving the computer's hardware, software, and internal communications performance. Those system characteristics, especially the memory, system buses, hard disk and video cards, are unable to run as fast as processor themselves. As a consequence, processors may have to wait for the response from the system to send them data before moving on to complete the task. In those cases, increasing the processing performance will not change the overall system performance.

5.5.2 Gravitational Field Accuracy

Even though a given hybrid model may be computationally faster, it may also be less accurate. As a result, accuracy measurements are also computed.

Measurement

Each grid point is seperated in longitude and latitude by 5 degrees, or 10 degrees for 30 degree 30 order models. Also, the distance of each grid point from the origin of the planetocentric coordinate system is equal to the equatorial radius (RE) of the moon. The 5 and 10 degree separation in longitude and latitude takes into account the resolution effects of spherical harmonics. Setting the radius equal to RE, weighs the importance of matching each coefficient equally.

After the grid is charted, the gravitational acceleration vector, in a Euclidean basis, is computed using the primary spherical harmonic and hybrid models at each grid point. The percent difference or error between those two vectors at each grid point is calculated as seen in Equation 5.6. Equation 5.6 allows the error to take in account the differences in direction and magnitude.

$$Error = \left[\frac{\|\overline{a}_{PSH} - \overline{a}_{Hybrid}\|}{\|\overline{a}_{PSH}\|} * 100\% \right] \tag{5.6}$$

After the error at every grid point is computed , the average of that error is then calculated.

Acceptable Values

While the measurement of accuracy can be determined, the range of acceptable values needs to be specified. This is accomplished by reflecting on the purpose of the higher degree and order terms of the spherical harmonic model.

When the degree and order of the spherical harmonic model increases, the estimate of the gravitational acceleration improves. If the estimate of the coefficients is accurate, then the estimate will converge to the true gravitational acceleration.

However how much the estimate of the gravitational acceleration changes depends on the order and degree of the spherical harmonic model and the value of the respective coefficients. For example, for the earth, the contribution of the J2 coefficient significantly alters the gravitational acceleration than the other higher degree and order coefficients.

Hence, when one increases the order and degree of the spherical harmonic model, it is expected that the gravitational acceleration will change by some amount. And if the coefficients are accurate, that change will improve the estimate of the gravitational acceleration.

When supplanting the primary spherical harmonic model by the hybrid model, it is desired that the hybrid model will not change the gravitational acceleration. However, for cases where the accuracy is not exact, the hybrid model should not significantly alter the estimate in the gravitational acceleration.

In this case, according to Figure 5.2, the gravitational acceleration computed from the 8 degree 8 order spherical harmonic model is varied by on average 0.047% compared to the point mass gravity model. Likewise, increasing the degree and order of the spherical harmonic to the 15 degree 15 order, the gravitational acceleration varies by 0.055% compared to the point mass gravity model. In addition, for the 30 degree 30 order spherical harmonic model, the gravitational acceleration varies have a difference of 0.07% than the point mass gravity model.

Since the accuracy of the hybrid should not significantly effect the change in the gravitational acceleration, the average percent errors in the gravitational acceleration of the hybrid model needs must orders of magnitude smaller then the expected change in the gravitational acceleration. The changes in gravitational accelerations in Figure 5.2 are within the same order of magnitude as 0.01%. Based on that information, the upper bound on the acceptable error between the hybrid model and 8 degree 8 order, 15 degree 15 order and 30 degree 30 order primary spherical harmonic models was chosen, conservatively, to be 10^{-4}%. However, it is recommended that further studies be performed on refining the upper bound on the acceptable errors between the two models.

Accuracy of Mass Concentration Model

The accuracy of the hybrid model depends on the accuracy of the mass concentration model and the secondary spherical harmonic models. But, the secondary spherical harmonic model has the same mathematical structure and program as the primary spherical harmonic model. So, any assigned coefficients to the secondary spherical harmonic model from the primary spherical harmonic model will not produce any error in the gravitational acceleration between the primary and secondary spherical harmonic models.

Hence, inaccuracies in the hybrid model are due to errors in estimating the values of the
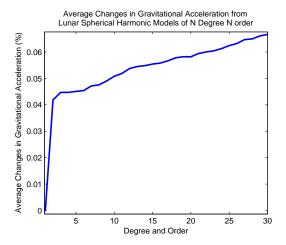
Figure 5.2: The y axis shows the percent difference between the average gravitational acceleration of the spherical harmonics at a given N degree and N order and the point mass gravity, 0 degree 0 order term. The gravitation accelerations were computed at 5 degree increments in latitude and longitude, with the radius at the surface of the moon. The x axis shows the value of N, the degree and order of the spherical harmonic model.

masses in the mass concentration model. As the mass concentration model is assigned more co-efficients from the primary spherical harmonic model, the accuracy of the hybrid model will, in general, decrease. The decrease in accuracy will continue until the mass concentration has all the coefficients of the primary spherical harmonic model, and the secondary spherical harmonic model is set to 0 degree 0 order.

So, the accuracy of the hybrid model hinges on the accuracy of the mass concentration model. If the mass concentration model performs poorly then the hybrid model will also perform poorly. Increasing the degree and order of the secondary spherical harmonic model will only help to alleviate the inaccuracy of the hybrid model.

5.5.3 Trajectories Errors

Besides using a gravity map to judge the accuracy of the hybrid model, trajectories can also describe the inaccuracies of the hybrid model. A given trajectory will be propogated with the true potential and the estimated potential. Afterwards, the maximum and minimum error in cross-track, altitude and down-range for a given duration is computed.

Trajectory Parameters

To narrow down the parameters of the trajectory, trajectories of the Lunar Prospector were

examined. Besides being a low orbiting satellite, Lunar Prospector's trajectory was designed to measure the gravitational acceleration of the moon. In doing so, the satellite orbited the moon primarily in a near circular polar orbit at 100 km altitude [32].

As a result, the satellites are initially in a 100 km circular orbit with a variable initial inclination. The circular orbit does not allow the errors between the two trajectories of the satellites governed by the spherical harmonics or the hybrid model to be heavily weighted by one region over the other as would be the case in more eccentric orbits. The variable initial inclination will allow a global sweep of trajectories about the moon to be generated.

The trajectory using the primary spherical harmonic and hybrid models was generated for 5 and 30 days. The 5 days allows for a short term error comparison, while the 30 days allows for a longer term comparison. Comparing trajectories for both time frames allows the growth rate of the error to be observed. In addition, 30 days was approximately when the lunar prospector initiated orbital corrections.

Trajectory Computations

First, the trajectory of one lunar satellite is computed using a hybrid model. Then, the trajectory of another satellite under the same initial conditions as the first is computed while implementing the primary spherical harmonic model.

Both trajectories are generated using Encke's method. Encke's method is sensitive to smaller perturbations, by avoiding truncation errors as a result of a limited computer word size. See reference [33] for more information.

After the trajectories were computed in lunar geocentric coordinates, those coordinates were transformed into local vertical local horizontal coordinates of the satellite. Afterwards, the distance between the positions of the satellites in cross-track, down-range, and altitude were computed.

Trajectory Nuances

There are some analysis issues. If the hybrid models performs poorly, the satellite governed by the hybrid model can crash into the moon. In addition, as the satellite approaches the mascons, the convergence rate of the simulation becomes poor. The simulation generating the trajectory of the satellites numerically integrates the velocity and position state variables. As the step size

becomes smaller, the numerical precision of the integration becomes better. Thus, a smaller step size is required.

Chapter 6

Results and Discussions

6.1 Preliminary Results

To understand the upcoming results better, additional studies on the effect of condition number and convergence on the accuracy of the mass concentration model were conducted.

6.1.1 Factors That Produce Poor Condition Number

Since poor condition number generates error in the estimation of the values for the masses in the mass concentration model, it is necessary to determine what factors, besides those mentioned already, contribute to ill conditioned coefficient and weight matrices.

In Figure 6.1 , those additional factors can be readily observed. First, the condition number of the ceofficient matrix in the mass estimation scheme grows when the masses in the mass distribution move closer to the origin. For example, in all three cases, the condition number increases as the masses move closer to the origin. That effect is a result of increasing similarity between columns of the coefficient matrix as the masses move towards the origin. As a result, the linear independence of the coefficient matrix becomes weaker leading to higher condition numbers.

Second, adding more masses in the configuration increases the condition number. Additional masses in the mass distribution results in more columns in the coefficient matrix. In addition, as the masses increase in number, the mass distribution becomes more congested leading to more similar columns in the coefficient matrix. Those two factors, increasing the size and reducing the linear independence of the coefficient matrix generates higher condition numbers.

Third, when the number of masses in the mass distribution was increased to 483, the condition number of the coefficient matrix started to become significant. As a result, the error in the mass estimation scheme became jagged after the masses in the mass distribution were relocated in a radial position after 0.2 RE. Therefore, if the condition number of the ceofficent matrix becomes significant, the errors will start to become jagged. In addition, the overall error will also increase in comparison to smaller mass distributions.
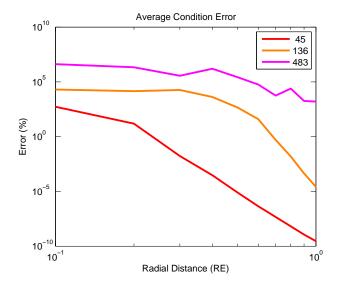
Figure 6.1: The mass configurations differed by the total number of masses. Except for the mass at the center, each mass in a configuration was displaced radially. After each displacement, the percent error in computing the inverse of the $J^T W J$ matrix was computed, see the vertical axis. In this case, the weight matrix was equalt to the identity matrix. The horizontal axis shows the radial position of the masses from the origin, in units of equatorial radius of the moon (RE).

6.1.2 Factors That Govern Convergence Errors

The convergence error can significantly affect the accuracy of the mass concentration model. For greater understanding of those factors, a test case was run. Unlike condition number, as the masses move towards the origin, the error in convergence decreases exponentially. The justification for this effect comes from examining the $\left(\frac{RE}{r}\right)^n$ factor. As the masses move away from the evaluation point, the $\left(\frac{RE}{r}\right)^n$ factor in the spherical harmonic expansion decreases the weight or influence of the higher order or degree terms in the spherical harmonic expansion. Hence, the inaccuracies of the higher order and degree terms become less influential.

Figure 6.2 also shows how the current procedures affect the convergence error. According to that procedure, the total number coefficients for each mass in a given mass concentration model is equal to the total or maximum coefficients of the primary spherical harmonic model. In addition, the number of masses in the mass distribution increases as the degree and order primary spherical harmonic model increases. Hence, as the masses increase in quantity, the number of coefficients in the coefficient matrix will also increase. According to the Figure 6.2, adding more masses will decrease the average convergence errors, resulting in more accurate mass concentration models.
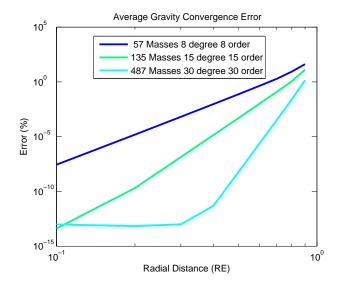
Figure 6.2: Except for the mass at the center, each mass in a configuration was displaced radially. After each displacement, the total number of coefficients in the coefficient matrix for each mass were set to 8, 15 or 30. Then, after estimating the mass values in the mass estimation scheme, the average error of the gravitational acceleration between the mass concentration model and its spherical harmonic equivalent was computed. The horizontal axis shows the radial position of the masses from the origin in units of equatorial radius of the moon (RE).

6.2   Potential Zeros Results

The potential zeros approach places the masses at the locations where the potential is equal to zero, see subsection 5.2.1 for more details.

6.2.1   8 Degree 8 Order Model

Uniformity Reconfigurations

The analysis of the mass concentration model using the potential zeros approach begins by examining the effect of the location of the masses. The distribution in latitude and longitude depends on the degree of the matching potential; but, that degree does not necessary have to be the maximum degree of the matching potential. Likewise, there is no indication of where the masses should be located radially within the sphere occupied by the potential source.

Radial Position Effect on Accuracy

So, see Figure 6.3, the first analysis was the effect of those characteristics on the accuracy of the mass distribution governed by the potential zeros approach for the 8 degree 8 order spherical
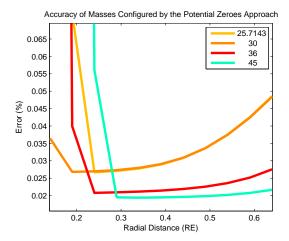
Figure 6.3: The matching degree was 7,6,5, and 4. The resulting distribution in longitude is displayed in the legend. The rest of the masses were uniformly distributed in latitude. There were 34 masses in the mass distribution for all four cases. The vertical axis shows the percent error between the mass concentration model and the primary spherical harmonic model. The horizontal axis shows the radial position of the masses from the origin, in units of equatorial radius of the moon (RE).

harmonic model.
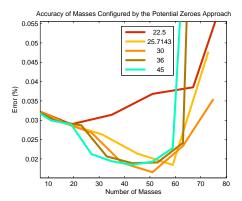
The accuracy of the mass distribution was affected by the position of the masses in longitude, and latitude. For example, there is 0.025% error between the masses distributed in longitude at 45 degrees and 25.71 degrees longitude.

The radial distance also contributed to the accuracy of the masses. The different mass configurations had their minimum error occurring at 0.25 RE to 0.3 RE. The condition number error starts to become significant before 0.2 RE to 0.3 RE. As the masses move away from 0.3 RE, the convergence error becomes larger leading to greater increases in error.

At what point the convergence and condition number errors start to become apparent depends on the uniformity of the masses in longitude. For example, at a separation of the masses at 45 degrees in longitude, the condition number errors starts to undermine the accuracy at a radius distance of 0.2 RE. However, when the masses are seperated by 30 degrees in longitude, the condition number errors becomes significant before 0.3 RE.

Mass Effect on Accuracy

Since the accuracy of the potential zeros approach was unsatisfactory, the total number of masses for the potential zeros approach was varied, see Figure 6.4. According to theory, as the
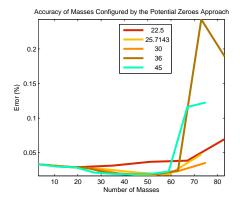
Figure 6.4: The quantity of the masses in the distribution was varied from 6 to 80. After computing the accuracy for five different configurations, as seen in Figure 6.3, the minimum error was recorded and plotted. The figure on the right shows the complete results while the figure on the left shows a magnification of the clustered region in the figure on the right. The vertical axis shows the percent error between the mass concentration model and the primary spherical harmonic model. The horizontal axis shows the radial position of the masses from the origin, in units of equatorial radius of the moon (RE).

masses in the mass distribution increase in quantity, the accuracy of the mass concentration model should improve.

However, as can be seen, after 60 masses in the mass distribution, the error increases dramatically. The condition of the coefficient matrix starts to become large enough to introduce error into the mass estimation model. As a consequence, adding more masses will not increase the accuracy of the mass concentration model.

When adding more masses in the distribution, the separation in longitude that produces the most accurate mass distribution varies. When 50 masses were separated by 30 degrees in longitude, the error in the mass concentration model reaches a global minimum. However, when the mass distribution had 30 masses, the best separation in longitude was 45 degrees.

In either case, the most accurate mass distribution had an error of 0.01%, which is more than 0.0001%, the upper limit for acceptable accuracy values. Hence, the potential zeros approach for the 8 degree 8 order could not generate an accurate mass distribution.

6.2.2   15 Degree 15 Order Model

Mass Effect on Accuracy

Like the 8 degree and 8 order case, see Figure 6.5, the accuracy of the mass concentration
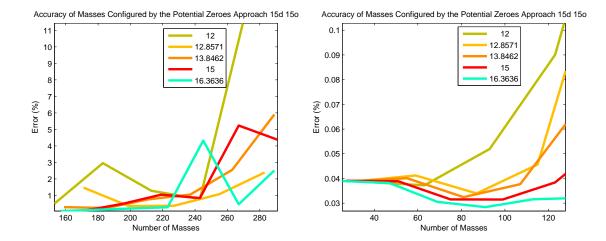
Figure 6.5: The number of masses was varied from 30 to 280. After computing the accuracy for the five different configurations, the minimum error was recorded and plotted. The vertical axis shows the percent error between the mass concentration model and the primary spherical harmonic model. The horizontal axis shows the radial position of the masses from the origin, in units of equatorial radius of the moon (RE).

was examined for a range of quantities and radial positions of masses. The distribution of the masses was configured using the potential zeros approach.

The 15 degree and 15 order hybrid mass concentration model can use more masses to achieve the same processing gains as in the 8 degree 8 order case. As consequence, the number of masses available to the mass concentration model increased from 56 to 296.

The accuracy of the mass concentration model should in theory improve as the masses increase. However, in this case, the most accurate mass distribution occurs when there are 90 masses. As the number of masses in the distribution is increased beyond that point, the error in the estimate of the values of the masses increases.

Beyond 120 masses, the condition number of the coefficient matrices becomes worse resulting in larger errors in estimating the mass values. If the mass configuration was not conditioned in order to mitigate the condition errors resulting from lack of independent columns in the coefficient matrix, the errors will be more significant and less continuous.

The accuracy of the model tends to improve as the locations of the masses in longitude become more spread out. Eventually, spreading out the masses in latitude will lead to a more condensed configuration in latitude. As those masses become closer to each other, the condition number will increase resulting in more error in the overall model.

Radial Position Effect on Accuracy

Like the 8 degree and 8 order case, see Figure 6.6, a sample of the accuracy of the mass concentration as one moved the masses from the origin was determined for 15 degree and 15 order case. The distribution of the masses was configured using the potential zeros approach. However, unlike the sample in the 8 degree 8 order case, this sample was a result of using the best mass configuration.

Except when the masses are distributed in longitude by 12 degrees, the other displacements in longitude produced smooth error curves indicating that the condition number error wasn't significant. Spreading out the masses by 12 degrees in longitude tends to poorly conditioned, as the masses are too close together.

In comparison to previous results, the best radial positions of the masses occurs at larger distances from the origin. For the 8 degree 8 order, the minimum error occured around 0.3 RE. However, for the 15 degree 15 order, the minimum error occured around 0.6 RE.

The general increase in error as the radial position of the masses increased is due to convergence errors.

In either case, the most accurate mass distribution resulted in about 0.03% error, more than 0.0001% error, the upper limit for acceptable accuracy values.
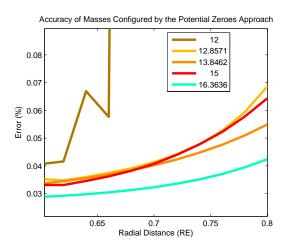
Figure 6.6: A sample of the best mass configurations for the potential zeros approach of the 15 degree and 15 order model. This figure only shows the region where the configuration error is minimal. 90 masses for the configuration was selected. The vertical axis shows the percent error between the mass concentration model and the primary spherical harmonic model. The horizontal axis shows the radial position of the masses from the origin, in units of equatorial radius of the moon (RE).

6.2.3   30 Degree 30 Order Model

Mass Effect on Accuracy

Like the 15 degree and 15 order case, the accuracy of the mass concentration was examined for a range of quantities, and radial positions of masses. The distribution of the masses was configured using the potential zeros approach.

The 30 degree and 30 order hybrid mass concentration model can use more masses to achieve the same processing gains as in the 15 degree 15 order case. As consequence, the number of masses available to the mass concentration model increased from 296 to 1022.

The best mass distributions occurs when the amount of the masses are 120 or 140. In theory, the best mass distribution should be at 1022 masses. However, the condition number error negates any accuracy gain by introducing more masses into the mass distribution, see Figure 6.7.

Like with the other cases, the placement in longitude and latitude has an effect on the average error of the mass concentration model. In addition, there is no absolute arrangement of the masses that will minimize the average error for a range of masses. Between 80 to 120 masses, the 45 degree placement of the masses in longitude had the most accurate mass distribution. However, that placement produced the least accurate mass distribution for mass distributions with more than 120 masses.
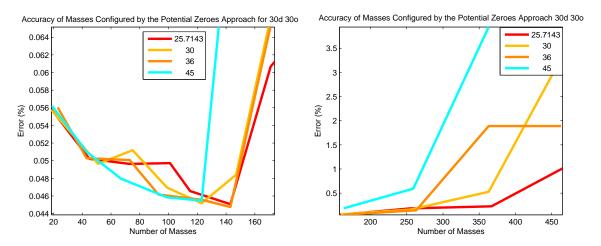
Figure 6.7: The masses were relocated in radial distance and in uniformity. The minimum errors in those re locations were plotted against the quantity of masses. The figure on the left shows the percent error for 20 to 180 masses. The figure on the right also displays the percent error for 180 to 453 masses. The vertical axis shows the percent error between the mass concentration model and the primary spherical harmonic model. The horizontal axis shows the radial position of the masses from the origin, in units of equatorial radius of the moon (RE).

Radial Position Effect on Accuracy

Like before, a sample of the accuracy of the mass concentration as one moved the masses from the origin was determined for 30 degree and 30 order case. The distribution of the masses was configured using the potential zeros approach. The sample was of the best mass configuration as seen in Figure 6.8.

Since the condition number error is too high, the trends in the errors for different separations in longitude are not smooth, resulting in jagged and somewhat unpredictable plots.

In comparison to samples for lower degree and order models, the most accurate mass distribution for the 30 degree 30 order occurs closer to the evaluation surface. That pattern is an effect of the condition number. As a mass distribution is relocated away from the origin, the condition number improves, resulting in more accurate estimates.

The most accurate mass distribution resulted in about 0.05% error, more than 0.0001% error, the upper limit for acceptable accuracy values.
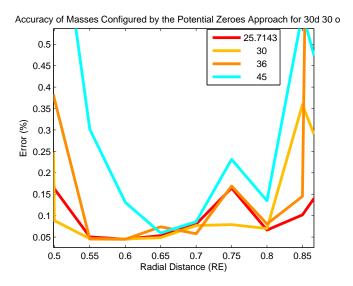
Figure 6.8: A sample of the best mass configuration for the 30 degree 30 order model. The vertical axis shows the percent error between the mass concentration model and the primary spherical harmonic model. The horizontal axis shows the radial position of the masses from the origin, in units of equatorial radius of the moon (RE).

6.3 Gravitational Anomalies Results

The gravitational anomalies approach places the point masses at the center of the gravitational anomalies, see subsection 5.2.2 for more details.

Latitude, Longitude, and Radial Displacements

The analysis of the mass concentration model using the gravitational anomalies approach begins by examining the effect of the location of the masses. It is uncertain whether or not placing a mass at the center of the gravitational anomaly at some radial distance will produce the most accurate mass distribution. Therefore, the displacements in latitude, longitude and radial distance of the entire mass distribution were studied.

6.3.1   8 Degree 8 Order Model

Latitude Displacements

The gravitational anomalies approach began by studying the effects of latitude displacement on the accuracy of the model.

According to Figure 6.9, relocating the masses by a negative degree in latitude results in more accurate mass distributions in comparison to displacing the masses by a positive degree in latitude. For example, when the masses were located at 0.8 RE from the origin, the masses displaced by -2 degrees latitude was 0.09% more accurate than masses relocated by 2 degrees in latitude.
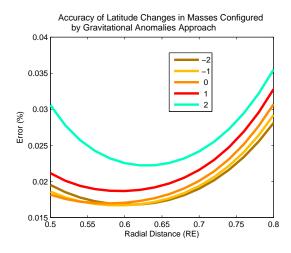
Figure 6.9: Except for the mass at the origin, every mass in the initial mass configuration was displaced in latitude and in radial position. The vertical axis shows the average percent error between the primary spherical harmonic model and the mass concentration model with the relocated mass distribution. The horizontal axis represents the radial position, in units of the radial equator of the moon, of the masses in the mass distribution.

The convergence errors begin to contribute to the error in the model as the masses move away from the origin. The condition errors remain small for the most part until the masses are

about 0.25 RE from the origin.

When the condition errors become influential, any relocation of the masses in latitude from their initial position tends to decrease the accuracy. At 0.6 RE, the most accurate mass configuration occurs at -1 degrees latitude.

Longitude Displacements

Like the latitude, the masses were first relocated in longitude by $\pm 4, \pm 2$ or 0 degrees. Afterwards, every mass had its radial position changed, see Figure 6.10.

The longitude displacements affect the overall accuracy of the mass distribution. Negative or zero longitude changes in the mass initial longitude location tend to increase the accuracy of the model in comparison to positive longitude displacements.

At some radial positions, one longitude displacement is better than another. Hence, there is really no absolute longitude displacement to achieve the most accurate mass distribution.
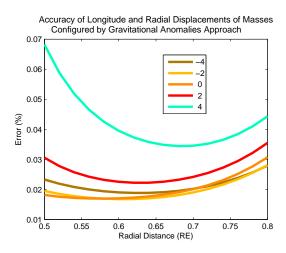
Figure 6.10: Except for the mass at the origin, every mass in the initial mass configuration was displaced in latitude and in radial position. The vertical axis shows the average percent error between the primary spherical harmonic model and the mass concentration model with the relocated mass distribution. The horizontal axis represents the radial position, in units of the radial equator of the moon, of the masses in the mass distribution.

There also appears to be no symmetry in the displacements in latitude or longitude. The 4 degrees in longitude and latitude does not have the same effect as the -4 degrees in longitude and latitude. Likewise, the 2 and -2 degrees are also dissimilar.

The most accurate mass distribution for displacements in latitude or longitude resulted in about 0.017 % error, more than 0.0001% error, the upper limit for acceptable accuracy values.

6.3.2   15 Degree 15 Order Model

Latitude Displacements

For the 15 degree 15 order model, the latitude and radial position of the initial mass configuration was varied, see Figure 6.11.

The displacements in latitude of the masses centered at the gravitational anomalies for the 15 degree and 15 order model influence the accuracy of the mass concentration model. The negative latitude relocations of the masses decreased the overall error in the model in comparison to other latitude displacements.

The radial distance where the minimum error occurs is farther out from the origin in comparison to the 8 degree 8 order case. The larger amount of masses in the mass distribution for the 15 degree 15 order case increases the condition number of the coefficient matrix leading to larger errors. Those errors are mitigated as the mass distribution increases its radial distance from the origin. As a result, the radial location of the minimum error is increased.
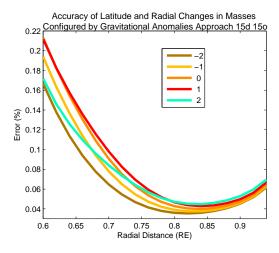
Figure 6.11: Except for the mass at the origin, every mass in the initial mass configuration was displaced in longitude and in radial position. The vertical axis shows the average percent error between the primary spherical harmonic model and the mass concentration model with the relocated mass distribution. The horizontal axis represents the radial position, in units of the radial equator of the moon, of the masses in the mass distribution.

Longitude Displacements

For the 15 degree 15 order model, the longitude and radial position of the initial mass configuration was altered, see Figure 6.12. Like the latitude displacements, negative longitude

relocations of masses generally produced more accurate mass concentration models. Unlike the latitude displacements, the range of errors for the longitude rearrangements of the masses is larger.

Similar to latitude, the longitude displacements show the radial location where the minimum error occurs moving farther away from the origin. In addition, the longitude and latitude displacements do agree that the best radial location is around 0.8 RE.

The most accurate mass distribution for displacements in latitude or longitude resulted in about 0.04% error, more than 0.0001% error, the upper limit for acceptable accuracy values.

In comparison the 8 degree 8 order case, the longitude and latitude for the 15 degree 15 order case had a smaller error range. The different relocations in longitude and latitude did not have a significant effect as 8 degree 8 order. In addition, the radial position of the most accurate mass distribution for 15 degree 15 order model was further away from the origin than the radial position of the most accurate mass distribution for the 8 degree 8 order model.
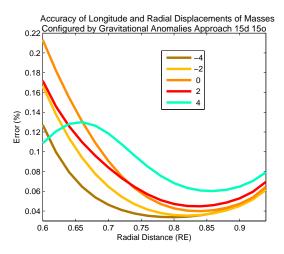
Figure 6.12: Except for the mass at the origin, every mass in the initial mass configuration was displaced in latitude and in radial position. The vertical axis shows the average percent error between the primary spherical harmonic model and the mass concentration model with the relocated mass distribution is computed and plotted. The horizontal axis represents the radial position, in units of the radial equator of the moon, of the masses in the mass distribution.

6.3.3   30 Degree 30 Order Model

Latitude Displacements

In the case of the 30 degree 30 order model, the latitude and radial position of the initial mass configuration was varied, see Figure 6.13. Unlike the previous cases, the displacements in
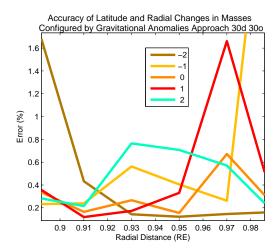
Figure 6.13: Except for the mass at the origin, every mass in the initial mass configuration was displaced in latitude and in radial position. Since the variance in error is rather large, the figure only shows the most accurate results. The vertical axis shows the average percent error between the primary spherical harmonic model and the mass concentration model with the relocated mass distribution is computed and plotted. The horizontal axis represents the radial position, in units of the radial equator of the moon (RE), of the masses in the mass distribution.

latitude are no longer as smooth. The larger coefficient matrices increase the condition error resulting in poorer and sensitive estimates of the mass values for the mass distribution.

When the radial position of the masses changes, the condition number is altered. However, since the condition number is so large, those changes in condition number are reflected in the jagged lines.

The convergence error at this point does not overshadow the condition errors in the model, since the 30 degree and 30 order is sufficient for proper convergence (see Figure 6.2 and Figure 6.1) As a result, the minimum error occurs near the evaluation surface, a region dominated in smaller models by the convergence errors.

Longitude Displacements

For the 30 degree 30 order model, the longitude and radial position of the initial mass configuration was altered.

The longitude displacements provide additional evidence that the condition number is hindering the mass estimation scheme from working properly. The jagged lines demonstrate that condition number is too large, and the variance of that error is significant and unpredictable, see Figure 6.14.
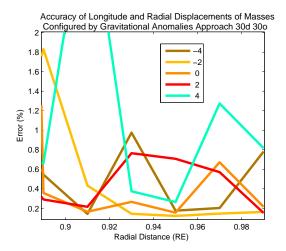
Figure 6.14: Except for the mass at the origin, every mass in the initial mass configuration was displaced in longitude and in radial position. Since the variance in error is rather large, the figure only shows the most accurate results. The vertical axis shows the average percent error between the primary spherical harmonic model and the mass concentration model with the relocated mass distribution. The horizontal axis represents the radial position, in units of the radial equator of the moon, of the masses in the mass distribution.

While not shown, if the radial distance from the origin gets closer to the origin, the error increases significantly. In addition, adding more masses will lead to higher condition numbers, resulting in more error in the model.

The longitude and latitude do not show significant difference for the 30 degree 30 order. In both results, the jagged nature of the error makes to difficult to predict the error for a given displacement in the mass distribution.

The most accurate mass distribution for displacements in latitude or longitude resulted in about 0.017% error, more than 0.0001% error, the upper limit for acceptable accuracy values.

6.4   Iterative Results

With a conditioned initial mass distribution, the iterative approach uses Matlab built in *fmincon* function to minimize the error in the mass concentration model, see subsection 5.2.3 for more details. Like the potential zeros approach, the number of masses for the initial mass distribution is a free parameter. For the iterative approach, the number of masses in the mass distribution was chosen in order for the hybrid model to achieve a certain computation speed, see Table 5.2.

6.4.1   8 Degree 8 Order Model

The Mass Distribution of a Hybrid Model with 10% Faster Computation Speed

The constrained optimization approach for the 8 degree and 8 order model used Matlab built in minimization routine to generate the best mass configuration. Due to the processing speed characteristics of the 8 degree and 8 order mass concentration model with 8 degree 0 order primary spherical harmonic model, 20% processing gain was unavailable. Hence, the 10% processing gain was selected, see Figure 6.15.

The constrained optimization generated a mass configuration that had 0.022% error. After 13 iterations, the final mass configuration occurred at 0.018%. In the aftermath, the additional iterations only improved the initial mass configuration by 0.004%.
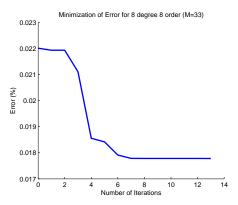
Figure 6.15: The numbers of masses in the configuration was set to 33, with an displacement of 0.4 RE and 0.5 RE. The constraints on longitude and latitude were respectively between 0 to 360, and -90 to 90. The radial constraints were from 0.2 RE to 0.95 RE. Each mass configuration was conditioned to alleviate condition number errors. The vertical axis shows the average percent error between the 8 degree 8 order primary spherical harmonic model and the mass concentration model with the relocated mass distribution. The horizontal axis represents the iterations of the *fmincon* program.

The Mass Distribution of a Hybrid Model with 5% Faster Computation Speed

The number of masses in the mass concentration model were increased to 57, resulting in an overall the 5% processing gain of the hybrid model, see Figure 6.16.

The additional masses did increase the accuracy of the mass concentration model. After 26 masses were added to the mass distribution, the final error improved by 0.003%. That increase

in accuracy, however, was not significant enough to decrease the error in the mass concentration model.

The most accurate mass distribution for 8 degree 8 order has 0.014% error, more than 0.0001% error, the upper limit for acceptable accuracy values.
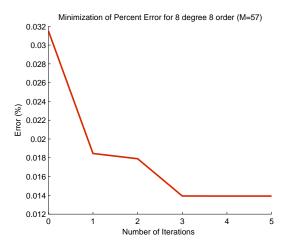

Figure 6.16: The number of masses in the configuration was set to 57, with an displacement of 0.4 RE and 0.5 RE. The constraints on longitude and latitude were respectively between 0 to 360, and -90 to 90. The radial constraints were from 0.2 RE to 0.95 RE. Each mass configuration was conditioned to alleviate condition number errors. The vertical axis shows the average percent error between the 8 degree 8 order primary spherical harmonic model and the mass concentration model with the relocated mass distribution. The horizontal axis represents the iterations of the *fmincon* program.

6.4.2   15 Degree 15 Order Model

The Mass Distribution of a Hybrid Model with 20% Faster Computation Speed

The iterative approach for the 15 degree 15 order mass concentration model started with examining a mass configuration such that the overall processing speed was 20% faster than the primary spherical harmonic model. However, the results from the iterative matlab showed no or very little improvement in the error of the mass concentration model.

The Mass Distribution of a Hybrid Model with 10% Faster Computation Speed

The processing speed was set to 10% resulting in a more massive mass concentration model.

The number of iterations was less than number of iterations of 5 and 14 in the 8 degree 8 order case. For, Figure 6.17 shows only 2 iterations.

The lack of iterations is probably due to the inital mass distribution being preconfigured to minimize errors in condition number and convergence. In addition, the 15 degree 15 order also decreases the amount of acceptable mass distributions, since the condition number error has started to become significant.
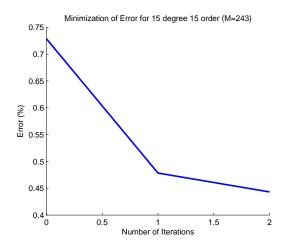
Figure 6.17: The fmincon matlab program was run with the 243 masses. The masses are relocated in radial distance only. The distribution of the masses in longitude and latitude are evenly distributed. The vertical axis shows the average percent error between the 15 degree 15 order primary spherical harmonic model and the mass concentration model with the relocated mass distribution. The horizontal axis represents the iterations of the *fmincon* program.

The Mass Distribution of a Hybrid Model with 5% Faster Computation Speed

Like the processing gain for 20%, the iterative approach did not improve upon the initial error in the mass distribution. The error of that distribution was at 0.2%.

Since the error did not improve significantly, the masses must be at their optimal locations.

The most accurate mass distribution for 15 degree 15 order has 0.02 % error, more than 0.0001 % error, the upper limit for acceptable accuracy values.

6.4.3 30 Degree 30 Order Model

Since the computation time increases approximately quadratic per parameter, the mass quantities were set to 135 and 145. According to the potential zeros approach, 135 and 145 were number of masses in the most accurate mass distributions.

135 Masses

The 135 masses in the mass distribution resulted in a nearly constant error of 0.12% despite three iterations. Since the iterations did not improve the error, the mass distribution must have been already at its optimal location. In addition, the effect of condition number on the error must be decreasing the set of acceptable mass distributions.

147 Masses

Like the 135 masses, there was no significant improvement on the initial error. The error in this case was also around 0.07%.

Both cases showed that the initial mass configuration was near the best location. That result can be explained by examining how the initial mass distribution was determined. The initial mass distribution was configured in such a way that the error in the mass estimation scheme from condition number and convergence was minimized. As a result, the optimization program did not significantly improve the error in the initial mass distribution of the mass concentration model.

The most accurate mass distribution for 30 degree 30 order had 0.07% error, more than 0.0001% error, the upper limit for acceptable accuracy values.

6.5   Similar Spherical Harmonic Models

This section explores whether or not another spherical harmonic model can perform as well as the hybrid model in replicating the primary spherical harmonic model and modeling the true gravitational acceleration.

8 Degree 8 Order

As seen in Table 6.1, all three hybrid models were not able to replicate the same gravitational acceleration as computed from a 8 degree 8 order model. In comparison to the true gravitational acceleration, a similar spherical harmonic model with an approximately equivalent computation speed is more accurate than 2 out of the 3 hybrid models. In addition, a similar spherical harmonic model that is approximately as accurate as hybrid model has a higher computation speed in all three cases.

Table 6.1: The third row from the top is the primary spherical harmonic model. The P,G, and I in the approach column represents respectively the potential zeros approach, gravitational anomalies approach, and iterative approach. The replicate category under the error column shows the error in replicating the primary spherical harmonic model, while the true category under the error column is the error between the hybrid or primary spherical harmonic model and the true gravitational model, considered to be a 30 degree 30 order spherical harmonic model. The similar spherical harmonic column displays the closest spherical harmonic model in accuracy or computation speed for a given hybrid model.

	Mass Concentration		Spherical Harmonics		Error %		Similar Spherical Harmonic Model			Hybrid Models' Computation	Similar Spherical Harmonic Model		
	Number of Masses	Approach	Degree	Order	Replicate	True	Equivalent Computation Speed				Equivalent Error		
Primary			8	8	0	0.0481	True Error %	Degree	Order	Speed %	Speed %	Degree	Order
Hybrid Models	53	P	7	0	0.0191	0.0516	0.0494	8	4	2.51	15.9	4	3
	31	G	7	0	0.0130	0.0508	0.0530	8	2	4.43	7.71	6	3
	57	I	7	0	0.0146	0.0505	0.0494	8	4	1.99	9.31	6	4

15 Degree 15 Order

As shown in Table 6.2, the hybrid models are not as accurate as the primary spherical harmonics. However, a spherical harmonic model with a similar computation speed has a higher true error for the mass concentrations model with the gravitational anomalies approach and the iterative approach. Another spherical harmonic model with almost equivalent true error in comparison to the hybrid models has a slower computation speed.

30 Degree 30 Order

As displayed in Table 6.3, since the true gravitational acceleration is considered to be a 30 degree 30 order model, the error in replicating the primary spherical harmonic model is equal to the error in matching the true gravitational acceleration. In all three hybrid models, the similar spherical harmonic models has a faster computation speed, and better accuracy. The condition number's effect on the poor inaccuracy of estimating the mass values for the mass distribution leads to significant errors.

6.6   Accuracy Reconsiderations

Since the accuracy of the potential zeros, gravitational anomalies and iterative approaches

Table 6.2: The third row from the top is the primary spherical harmonic model. The P,G, and I in the approach column represents respectively the potential zeros approach, gravitational anomalies approach, and iterative approach. The replicate category under the error column shows the error in replicating the primary spherical harmonic model, while the true category under the error column is the error between the hybrid or primary spherical harmonic model and the true gravitational model, considered to be a 30 degree 30 order spherical harmonic model. The similar spherical harmonic column displays the closest spherical harmonic model in accuracy or computation speed for a given hybrid model.

	Mass Concentration		Spherical Harmonics		Error %		Similar Spherical Harmonic Model			Hybrid Models' Computation	Similar Spherical Harmonic Model		
	Number of Masses	Approach	Degree	Order	Replicate	True	Equivalent Computation Speed				Equivalent Error		
Primary			15	15	0	0.0391	True Error %	Degree	Order	Speed %	Speed %	Degree	Order
Hybrid Models	91	P	15	0	0.0348	0.0517	0.0460	9	6	27.2	34.0	7	2
	70	G	15	0	0.0242	0.0466	0.0481	8	8	29.9	27.1	9	5
	135	I	15	0	0.0223	0.0464	0.0468	11	4	23.4	21.0	12	3

Table 6.3: The third row from the top is the primary spherical harmonic model. The P,G, and I in the approach column represents respectively the potential zeros approach, gravitational anomalies approach, and iterative approach. The replicate category under the error column shows the error in replicating the primary spherical harmonic model, while the true category under the error column is the error between the hybrid or primary spherical harmonic model and the true gravitational model, considered to be a 30 degree 30 order spherical harmonic model. The similar spherical harmonic column displays the closest spherical harmonic model in accuracy or computation speed for a given hybrid model.

	Mass Concentration		Spherical Harmonics		Error %		Similar Spherical Harmonic Model			Hybrid Models' Computation	Similar Spherical Harmonic Model		
	Number of Masses	Approach	Degree	Order	Replicate	True	Equivalent Computation Speed				Equivalent Error		
Primary			30	30	0	0	True Error %	Degree	Order	Speed %	Speed %	Degree	Order
Hybrid Models	143	P	30	0	0.0452	0.0452	0.0440	11	10	57.7	60.1	10	10
	238	G	30	0	0.1203	0.1203	0.0498	19	1	49.9	n/a	n/a	n/a
	147	I	30	0	0.0649	0.0649	0.0459	12	4	56.7	75.1	0	0

did not achieve the desired level of accuracy, it was questioned whether or not the mass concentration model was producing the same inaccuracies as for other researchers.

6.6.1 Levie's Research

Out of the two researchers, Levie and McLaughlin, who worked with the mass estimation scheme, only Levie used the same scheme to replicate a potential. Unfortunately, Levie does not provide results showing the accuracy of his mass concentration model in the same way as presented in this document. However, using his masses values and configuration, and plugging them into the accuracy program resulted in the following.

In the Figure 6.18, the accuracy of Levie's work in replicating a lunar potential, would also fail to be within tolerable limits. The average error is around 0.02% which is higher than 0.0001%, the amount of change to the point mass gravitational acceleration when extending the spherical harmonic model to 3 degree 3 order. While there are some regions where the accuracy may be within the tolerance, those regions are somewhat small in comparison to the rest of the surface.
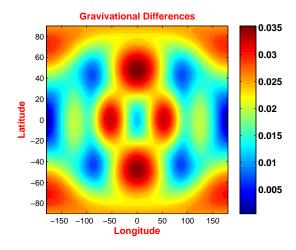
Figure 6.18: Accuracy of Levie's Work. A gravitational acceleration, as indicated in the colorbar, of the lunar surface indicating the errors (% increase) between the mass concentration model and the lunar potential. The vertical axis is the latitude and the horizontal axis is the longitude. Both longitude and latitude are in degrees.

6.6.2 Accuracy Surface Metrics

Since Levie's results were inaccurate, it was considered that the accuracy measurement might be too conservative. The evaluation at the surface of the moon equally weighs each coefficient. However, at evaluation surfaces with a non-zero altitude, the Stokes coefficients are reduced by a

factor of $\left(\frac{RE}{r}\right)^n$. As a consequence, the inaccuracies of mass concentration model in matching higher degree and order terms will have a less of an effect.

8 Degree 8 Order Model

From that perspective, the Figure 6.19 was generated. The accuracy of the hybrid model does improve as the radial distance of the evaluation surfaces increases. This is a result of the point mass gravity term becoming more influential in the gravitational acceleration at the evaluation surfaces. Since the mass concentration model does accurately model that point mass term, the inaccuracies of the mass distribution on other terms becomes less significant.
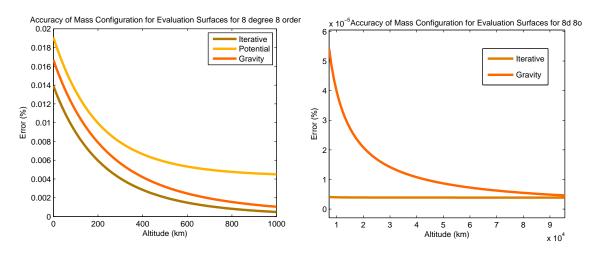
Figure 6.19: For the best three mass configurations, the vertical axis shows the percent error between the mass concentration model and the primary spherical harmonic model when computed at evaluation surfaces that varied in altitude. For the iterative and potential mass configurations, the number of masses were 56 and 57 respectively. The gravitational anomalies configuration was made up of 33 masses. The difference betwen the figures is the range in altitudes. The figure on the right does not include a mass distribution from the potential zeros approach, because the error was significantly larger than the iterative and gravitational anomalies approach.

However, despite the additional help, only the iterative and gravitational anomalies configurations on average were more accurate then 0.0001% only when the evaluation surfaces were above 1000 km.

The figure also shows how accurate each approach is in compared to each other. For example, the potential zeros approach is not as accurate as the gravitational anomalies even though the potential zeros approach has 32 more masses. The iterative approach is the most accurate, but it has 33 more masses than the gravitational anomalies approach.

15 Degree 15 Order Model

Like the 8 degree 8 order model, the best mass configuration for the iterative, potential zeros, and gravitational anomalies were selected based on the results provided in the previous sections.

The iterative approach produced the most accurate mass configuration, see Figure 6.27. That iterative approach, though, had more masses than the gravitational anomalies and potential zeros approach.

The accuracy of the models improves as the evaluation surface increases. However, since the mass configuration do not exactly estimate the mass point gravity, the error of the models does not converge to zero as the altitude of the evaluation surface goes to infinity. This is a result of the previous mass distribution not entirely satisfying the mass point gravity and other stronger terms.
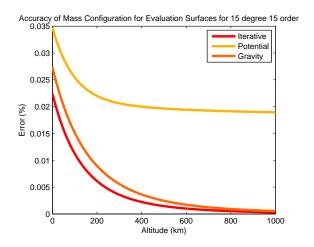
Figure 6.20: For the best three mass configurations, the vertical axis shows the percent error between the mass concentration model and the primary spherical harmonic model, computed at evaluation surfaces that varied in altitude. For the iterative and potential mass configurations, the total number of masses were 257 and 90, respectively. The gravitational anomalies configuration was made up of 137 masses.

30 Degree 30 Order Model

Like before, the best mass distributions were selected. However, unlike before, the best mass distribution from the iterative approach wasn't always the most accurate. Depending on the altitude of the evaluation surface, either the potential zeros approach or the iterative approach had the most accurate mass distribution, see Figure 6.21.
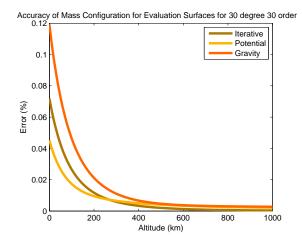
Figure 6.21: For the best three mass configurations, the vertical axis shows the percent error between the mass concentration model and the primary spherical harmonic model when computed at evaluation surfaces that varied in altitude. The altitude of the evaluation surface was increased from 0 to 1000 km.

At 1000 km, the errors in the mass distributions converge within the same order of magnitude of 0.0001%. The bias in the error is a result of the mass distribution not perfectly estimating the mass point gravity term.

6.7   Trajectory Error Analysis

After the three different approaches to determine the mass distribution for the mass concentration model were evaluated, the best configuration for the 8 degree 8 order, 15 degree and 15 order, and 30 degree and 30 order was selected for further testing.

6.7.1   8 Degree 8 Order model

For reference purposes, there are two cases considered. Both cases have an 8 degree 0 order secondary spherical harmonic model with the 8 degree 8 order mass concentration model. However, the first hybrid case has the masses configured using the iterative approach. The second hybrid case uses the gravitational anomalies approach to determine the properties of the masses, see Figure 6.22.

Cross-Track

The first hybrid case was slightly more accurate than the second hybrid case. The range of errors for the second hybrid case was $\pm 2 \times 10^4$ meters while the range of errors for the first hybrid
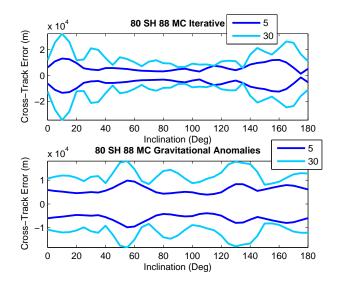
Figure 6.22: The vertical axis shows the maximum and minimum of the trajectory errors between the hybrid model and primary spherical harmonic model for a range of initial inclinations. The legend shows the duration of the trajectory, the first being 5 days and the second being 10 days. In both cases, the secondary spherical harmonics is 8 degree 0 order and the mass concentration is 8 degree 8 order. The first hybrid case used the iterative approach to configure the locations of the masses. The second hybrid case used gravitational anomalies approach to locate the masses.

case was $\pm 2.5 \times 10^4$ meters.

In both the first and second hybrid cases, there are inclinations where the cross-track did not grow significantly from 5 to 30 days. Those inclinations for the first case are 130, and for the second case is 175. Hence, for longer flight times, setting the satellites initial inclination at those values will help to stabilize the growth in error in cross-track.

Down-Range

Like before, both hybrid cases have similar down-range error, see Figure 6.23. The first case performs better on average except for inclinations around 180 degrees. That indicates that even though a hybrid case works well for a given range of inclinations, that hybrid case could possibly fail at other inclinations. Hence, to assure that the hybrid model is accurate, all inclinations must be examined.

In both hybrid cases, there are regions where the growth in the down-range primarily increases in one direction. For the first case, inclinations of 50 to 100, and 130 to 180 are regions where the growth occurs in one direction. Likewise, for the second case, those inclinations are 0 to 110, and 130 to 180 degrees.
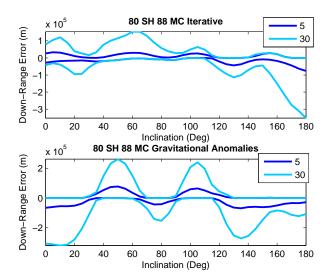
Figure 6.23: The vertical axis shows the maximum and minimum of the down-range trajectory errors between the hybrid model and primary spherical harmonic model for a range of initial inclinations. The legend shows the duration of the trajectory, the first being 5 days and the second being 10 days. In both cases, the secondary spherical harmonics is 8 degree 0 order and the mass concentration is 8 degree 8 order. The first hybrid case used the iterative approach to configure the locations of the masses. The second hybrid case used gravitational anomalies approach to locate the masses.

Altitude

Unlike the errors in down-range and cross-track, the altitude errors show that the second hybrid case is more accurate then the first hybrid case, see Figure 6.24. As a result, even though a hybrid case may be accurate in down-range and cross track, that hybrid case may have altitude errors.

The second hybrid case also has more stable inclinations, where the error growth rate is small in comparison to other inclinations.

6.7.2 15 Degree 15 Order Model

For reference purposes, there are two cases considered. Both cases have a 15 degree 0 order secondary spherical harmonic model with the 15 degree 15 order mass concentration model. However, the first hybrid case has the masses configured using the iterative approach. The second hybrid case uses the gravitational anomalies approach to determine the locations of the masses.

Cross-Track

The first hybrid case is more accurate than the second hybrid case, see Figure 6.25. However,
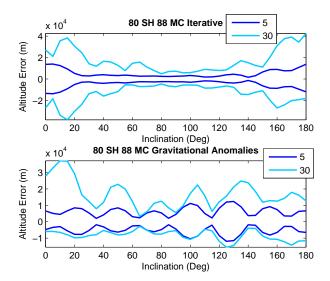
Figure 6.24: The vertical axis shows the maximum and minimum of the altitude trajectory errors between the hybrid model and primary spherical harmonic model for a range of initial inclinations. The legend shows the duration of the trajectory, the first being 5 days and the second being 10 days. In both cases, the secondary spherical harmonics is 8 degree 0 order and the mass concentration is 8 degree 8 order. The first hybrid case used the iterative approach to configure the locations of the masses. The second hybrid case used gravitational anomalies approach to locate the masses.
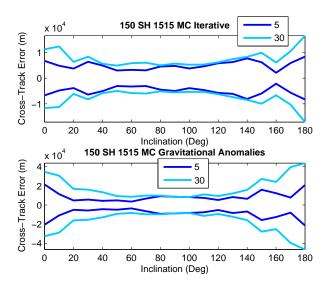
Figure 6.25: The vertical axis shows the maximum and minimum of the cross-track trajectory errors between the hybrid model and primary spherical harmonic model for a range of initial inclinations. The legend shows the duration of the trajectory, the first being 5 days and the second being 10 days. In both cases, the secondary spherical harmonics is 15 degree 0 order and the mass concentration is 15 degree 15 order. The first hybrid case used the iterative approach to configure the locations of the masses. The second hybrid case used gravitational anomalies approach to locate the masses.

the second hybrid case has more stable inclinations. Therefore, it not always true that the hybrid case with the minimal error will have the most stable inclinations.

Down-Range

The first hybrid case is slightly more accurate than the second hybrid case, see Figure 6.26. In addition, both cases show growth in the downrange occurring in one direction depending on the inclination.

Even though the growth in downrange occurs in one direction, there is not a general pattern relating the inclinations to the directions in growth. Hence, for at least the 15 degree 15 order, predicting the downrange error will be difficult.
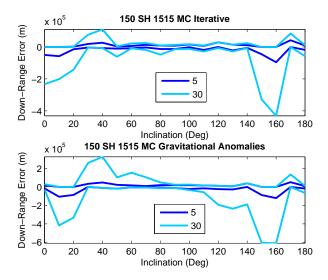
Figure 6.26: The vertical axis shows the maximum and minimum of the down-range trajectory errors between the hybrid model and primary spherical harmonic model for a range of initial inclinations. The legend shows the duration of the trajectory, the first being 5 days and the second being 10 days. In both cases, the secondary spherical harmonics is 15 degree 0 order and the mass concentration is 15 degree 15 order. The first hybrid case used the iterative approach to configure the locations of the masses. The second hybrid case used gravitational anomalies approach to locate the masses.

Altitude

Like the errors in down-range and cross-track, the first hybrid case is more accurate than the second hybrid case, see Figure 6.27. In both cases, there is a large increase in error at 150 degree inclinations. That implies that both hybrid models are unable to estimate the gravitational field within inclinations of 150 degrees.
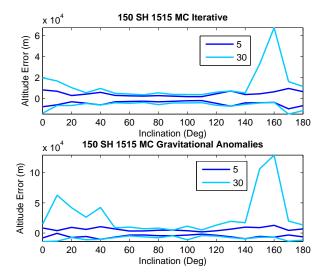
Figure 6.27: The vertical axis shows the maximum and minimum of the altitude trajectory errors between the hybrid model and primary spherical harmonic model for a range of initial inclinations. The legend shows the duration of the trajectory, the first being 5 days and the second being 10 days. In both cases, the secondary spherical harmonics is 15 degree 0 order and the mass concentration is 15 degree 15 order. The first hybrid case used the iterative approach to configure the locations of the masses. The second hybrid case used gravitational anomalies approach to locate the masses.

6.7.3   30 Degree 30 Order Model

Instead of using the best two mass configurations from two different approaches, the trajectory analysis examined the error of two different hybrid cases of a mass distribution close to the most accurate model. Examining the two different hybrid models will allow for greater insight into the accuracy improvement when changing the degree and order of the coefficients used in the secondary spherical harmonic model.

Like before, the trajectory errors were computed between the hybrid and the primary spherical harmonic model. The errors in cross-track, down-range, and altitude are shown in the following figures.

Cross-Track

The hybrid configuration where the secondary spherical harmonic model only modeled the coefficients composed of 27 degree 0 order resulted in more accurate model, see Figure 6.28. That hybrid configuration had errors of 10^4, one magnitude less then the errors in the second hybrid model, 28 degree 0 order secondary spherical harmonic model with the same 30 degree 30 order mass concentration model. Hence, it will not always be the case that increasing the degree of the
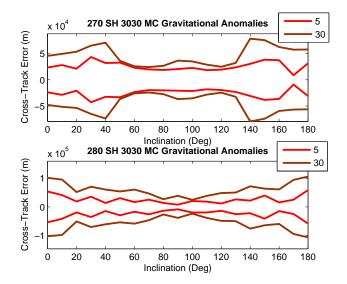
Figure 6.28: The maximum trajectories errors in down range for two different hybrid cases, for 180 degree range of inclination and for a flight time of 5 and 30 days. The figure on the top is the hybrid case where the secondary spherical harmonic model was 27 degree 0 order model. On the other hand, the figure on the bottom has secondary spherical harmonic model is 28 degrees 0 order. In both cases, the mass concentration model had the same mass configuration, but with different masses values due to the estimation scheme.

secondary spherical harmonic will lead to a more accurate hybrid model.

The second hybrid model has more stable points, where the trajectory errors do not significantly larger in time. For inclinations of 60 and 120, for example, the trajectory error for 5 days of flight time is close to the same trajectory computed for the 30 days of flight time. Those inclinations demonstrate that hybrid model can be used for at least month without significant growth in the cross track error.

Down-Range

The down-range trajectories also reconfirm that the hybrid case with the 27 degree 0 order secondary spherical harmonic model is more accurate than the 28 degree 0 order secondary spherical harmonic model. In addition, the difference in errors is about the same order of magnitude, see Figure 6.29.

The down-range in both hybrid models is increasing in one direction for a small range in inclinations. For example, the maximum down-range error for the first hybrid case at inclinations from 150 to 180 does not significantly change. However, the minimum downrange at those inclinations does grow in the negative direction.
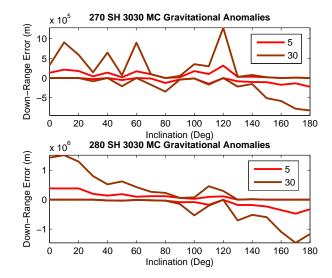
Figure 6.29: The maximum trajectories errors in cross track for two different hybrid cases, for 180 degree range of inclination and for a flight time of 5 and 30 days. The figure on the top is the hybrid case where the secondary spherical harmonic model was 27 degree 0 order model. On the other hand, the figure on the bottom has secondary spherical harmonic model is 28 degrees 0 order. In both cases, the mass concentration model had the same mass configuration, but with different masses values due to the estimation scheme.

Closer examination reveals that the down-range error grows in one direction only at equatorial orbits and small inclinations. If the specific momentum of the satellite is pointed in the positive direction, the down-range error will grow in the positive downrange direction. Likewise, if the specific momentum of the satellite is pointed in the negative direction, then the error in down-range will grow in the negative direction. Hence, for orbits about the equator, there is a correlation between the specific momentum vector and the direction of growth in the down-range error.

Altitude

Unlike the errors in down-range and cross-track, the error in altitude is similar for the first and second hybrid case. The first hybrid case is meters more accurate then the second hybrid case, instead of being an order of magnitude different, see Figure 6.30.

There are few stables or little to no growth in the altitude of the two different cases. For the first case, inclinations around 90 degrees have no significant growth in altitude. The second hybrid case has no significant growth in error for inclinations around 90 degrees. In both cases, initializing the satellite in a polar orbit increases the accuracy of the hybrid model.
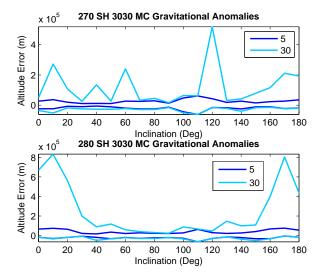
Figure 6.30: The maximum trajectories errors in cross track for two different hybrid cases, for 180 degree range of inclination and for a flight time of 5 and 30 days. The figure on the top is the hybrid case where the secondary spherical harmonic model was 27 degree 0 order model. On the other hand, the figure on the bottom has secondary spherical harmonic model is 28 degrees 0 order. In both cases, the mass concentration model had the same mass configuration, but with different masses values due to the estimation scheme.

In both the hybrid models, there is only significant growth of altitude error in the positive direction. This indicates that the trajectory of the satellite in a gravitational field described by the two different hybrid cases will tend to oscillate back and forth in altitude.

Chapter 7

Conclusions

After exploring the capabilities of the hybrid model in the previous results and discussions section, now the performance of the hybrid models can be evaluated. From that performance, conclusions can be drawn on the validity of the hybrid in replacing the primary spherical harmonic model.

7.1 Performance of 8 Degree 8 Order Hybrid Models

A summary of the computation speed and accuracy of various hybrid models for 8 degree 8 order is seen in Figure 7.1.

The hybrid models associated with the potential zeros approach had a larger average error than the hybrid models configured under the iterative and gravitational anomalies methods. In addition, the quickest hybrid model defined by the potential zeros approach and with the secondary spherical harmonic model at 3 degree 0 order was computationally slower than the most accurate hybrid models of the iterative or gravitational anomalies approaches.

On average, the hybrid models configured by the iterative approach is the most accurate. However, the gravitational anomalies method with a secondary spherical harmonic model at 7 degree 0 order generated the most accurate and quickest hybrid model.

7.2 Performance of 15 Degree 15 Order Hybrid Models

A summary of the computation speed and accuracy of various hybrid models for 15 degree 15 order is seen in Figure 7.2. Since the degree and order of the primary spherical harmonic model has increased to 15, there are more hybrid models with a faster computation speed than the 15 degree 15 order primary spherical harmonic model

The hybrid models configured by the potential zeros approach, in general, performs better than hybrid models using the gravitational anomalies approach. Nevertheless, the best hybrid
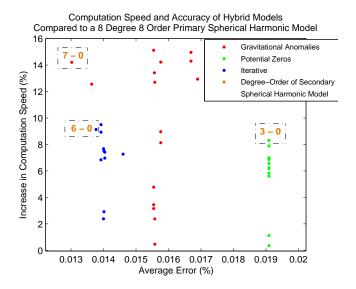
Figure 7.1: Computation speed and accuracy of hybrid models in replicating a 8 degree 8 order primary spherical harmonic model. The numbers in the dashed box indicate the degree and order of the secondary spherical harmonic model associated with the enclosed dotted marker.
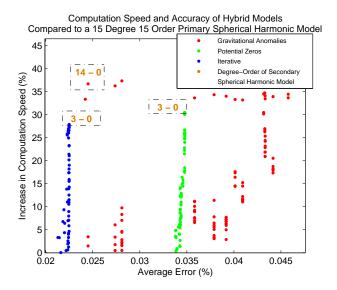
Figure 7.2: Computation speed and accuracy of hybrid models in replicating a 15 degree 15 order primary spherical harmonic model. The numbers in the dashed box indicate the degree and order of the secondary spherical harmonic model associated with the enclosed dotted marker.

model for the potential zeros approach with a secondary spherical harmonic model at 3 degree 0 order is less accurate and slower than the best hybrid models using the other two approaches.

On average, the iterative approach generated better hybrid models. However, the hybrid model configured by the iterative approach with a secondary spherical harmonic model at 3 degree 0 order is slightly more accurate but slower than the hybrid model with the gravitational anomalies approach and a secondary spherical harmonic model at 14 degree 0 order.

The errors due to high condition numbers of the coefficient matrix are starting to degrade the overall accuracy of the hybrid models.

7.3   Performance of 30 Degree 30 Order Hybrid Models

The computation speed and accuracy of various hybrid models were computed for 30 degree 30 order, as seen in Figure 7.3. Because the degree and order of the primary spherical harmonic model has increased to 30, there are more hybrid models with a faster computation speed than the 30 degree 30 order primary spherical harmonic model.

While there are more computationally faster hybrid models, the error in those hybrid models is increasing. The condition number of the coefficient matrices is becoming too large resulting in more significant poor estimates of the mass values in the mass estimation scheme for all three approaches.

Since the gravitational anomalies approach determined a mass distribution with 100 more masses than mass distributions generated by the iterative and potential zeros approach, the hybrid models defined by the gravitational anomalies approach is more susceptible to errors from high condition numbers. As a result, the hybrid models configured by the gravitational anomalies approach are more inaccurate than the hybrid models defined by the potential zeros and iterative approaches.

In this case, the hybrid models with the potential zeros approach are the most accurate. In addition, the hybrid model with a secondary spherical harmonic at 2 degree 0 order and the potential zeros approach is more accurate and quicker than the best hybrid models under the iterative and gravitational anomalies approaches.
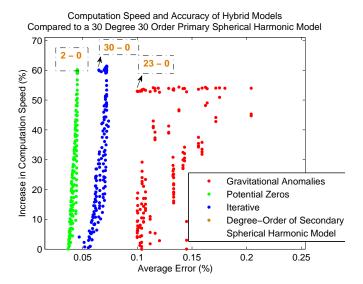
Figure 7.3: Computation speed and accuracy of hybrid models in replicating a 30 degree 30 order primary spherical harmonic model. The numbers in the dashed box indicate the degree and order of the secondary spherical harmonic model associated with the enclosed or pointed to dotted marker.

7.4 General Performance of the Hybrid Models

Besides separate conclusions for 8 degree 8 order, 15 degree 15 order and 30 degree 30 order, general conclusions of the hybrid model can be drawn based on Figures 7.1, 7.2 and 7.3.

In general for a given approach, as the degree and order of the spherical harmonic model increases, the accuracy of the hybrid model improves. However, at the same time, the computation speed of those models decreases.

The general performance of the hybrid models depends on the approach in generating the mass distribution, and the coefficients set aside for the secondary spherical harmonic model. For the most part, the gravitational anomalies approach generates the best hybrid model in replicating 8 degree 8 order, and 15 degree 15 order primary spherical harmonic models. On the other hand, for 30 degree and 30 order models, the best hybrid models is defined by the potential zeros approach.

While there are hybrid models that run faster than their primary spherical harmonic counterparts, they did not meet the accuracy requirements.

Chapter 8

Recommendations and Future Work

8.1 Alleviating Errors due to Poor Condition Number

A primary conclusion in this thesis was that poor condition number hindered the mass estimation scheme from working efficiently. Since the error due to condition number becomes worse after masses in the mass concentration model increase beyond or close to the number of coefficients in the matching potential, the mass concentration model cannot fully capture the accuracy benefits of increasing the masses in the mass distribution.

Hence, it is recommended that the mass estimation scheme (see Equation 4.18) be modified to eliminate the inverse of $J^T W J$. This can be accomplished by researching other ways to determine the mass values in an underconstrained system without using the least squares estimation approach. Another potential solution is to modify the iterative approach, by allowing Matlab's minimization program to also determine the mass values and their proper location with the objective function as the error between the coefficients or gravitational acceleration between the mass concentration and primary spherical harmonic model.

8.2 Fixing Convergence Errors

The convergence errors hindered the mass estimation scheme for small order and degree models, by restricting the masses to be closer to the origin. As the masses get closer to the evaluation surface, the convergence errors between the exact mass point equation and the spherical harmonic representation became larger, leading to more significant error between the estimated and true gravitational accelerations.

Fixing these errors can be accomplished by increasing the amount of coefficients given to each mass. Instead of setting the number of coefficients for each mass to equal the number of coefficients in the matching potential, more coefficients should be used. However, there is tradeoff since increasing those coefficients will increase the condition number of the coefficient matrix.

It is possible that changing the shape of the masses might help to increase the convergence rate. But, the gravitational acceleration equations for oblate and prolate spheroids require more processing time. Hence, if processing speed is a constraint, changing the masses' geometry lowers the amount of masses required to achieve a certain processing gain.

8.3 Software Investment

The analysis for this thesis used Matlab as the primary language and coding program. However, in most space applications, the onboard programs implement C or C++ due to being more efficient. For example, Matlab requires all libraries even though the program maybe using only a few, while C allows one to select the libraries reducing the amount of memory and processing inefficiencies.

Another key investment is that the processing speed of the spherical harmonics and mass concentrations models are different between Matlab 2010 and Matlab 2009. The Matlab 2010 actually improves the overall processing speed of the hybrid model. Hence, there was internal software development between the two versions which became advantageous for the processing speed of the hybrid model.

8.4 Hardware Investment

This thesis only examined the software implications of using the hybrid mass concentration and spherical harmonic models. However, the processing hardware can be reconfigured to increase the overall processing efficiency and speed of the hybrid model. Doing so, allows more masses to be used in the mass concentration model while maintaining a faster computation time for the hybrid model.

Modifying the hardware requires further research and study into the following: FPGYA processors, data storage such as floating point numbers, integer, decimal representation, and processing architecture.

8.5 Other Research Pursuits

Processing speed is not the only advantage in using mass concentrations instead of spherical harmonics. As stated in the literature survey, other researchers have used mass concentrations to estimate the mass flow rate for a given local region.

Mass concentrations can be used in a similar fashion. For example, the mass estimation scheme can estimate the variations in gravitational acceleration due to relocations, collisions or other manipulations of masses.

The mass concentration model can also be used to estimate variations of other potential due to changes in their potential sources. For example, if a segment of a satellite's exterior became electrically charged, the changes of the satellites magnetic and electric fields can be determined using the mass estimation scheme, where the masses values become electric charges.

References

[1] Roithmayr, C. M., "Contributions of Spherical Harmonics to Magnetic and Gravitational Fields," NASA/TM 213007, NASA, 2004.

[2] Junkins, J. L. and Schaub, H., *Analytical Mechanics of Space Systems*, AIAA Education Series, AIAA, Reston, Virginia, 2003.

[3] Pines, S., "Uniform Representation of the Gravitational Potential and Its Derivatives," *AIAA*, Vol. 11, No. 11, 1973, pp. 1508–1512.

[4] Barthelmes, F., "Definition of Functionals of the Geopotential and Their Calculation from Spherical Harmonic Models," Scientific technical report, ICGEM, Potsdam, Germany, September 2009.

[5] Lundberg, J. B. and Schutz, B. E., "Recursion Formulas of Legrendre Functions for Use with Nonsingular Geopotential Models," *Journal of Guidance*, Vol. 11, No. 1, Jan-Feb 1988, pp. 31–38.

[6] Gottlieb, R., "Fast Gravity, Gravity Partials, Normalized Gravity, Gravity Gradient Torque and Magnetic Field: Derivation, Code and Data," NASA Contractor Report 188243, NASA, Houston, 1993.

[7] Holmes-Siedle, A. G. and Adams, L., *Handbook of Radiation Effects*, Oxford University Press, Oxford, UK, 2002.

[8] Lowman, P., *Exploring Space Exploring Earth*, Cambridge University Press, Cambridge, UK, 2002.

[9] O'Hanlon, L., "Gravity Map Shows Earth Is Very Lumpy," Tech. rep., Discovery News, 2003.

[10] Baker, D., Allen, J., Kanekal, S., and Reeves, G., "Pager Satellite Failure May Have Been Related to Disturbed Space Environment," *Eos Transactions of American Geophysical Union*, Vol. 79, No. 40, October 1998, pp. 477.

[11] Kootnz, S., Pedley, M., and Mikatarian, R. R., "Materials Interactions with the Space Environment: International Space Station May 2000 to May 2002," *Protection of Materials and Structures from Space Environment*, Vol. 5 of *Space Technology Proceedings*, June 2004, pp. 31–72.

[12] Harland, D. M. and Lorenz, R., *Space System Failures*, Praxis Publishing Ltd., Berlin, Germany, 2005.

[13] Spieler, H., "Introduction to Radiation-Resistant Semiconductor Devices and Circuits," *AIP Conference Proceedings*, Vol. 390, 1997, pp. 23–49.

[14] Brown, C. D., *Elements of Spacecraft Design*, AIAA Education Series, AIAA, Reston, Virginia, 1st ed., 2002.

[15] Mayer, D. C. and Lacoe, R. C., "Designing Integrated Circuits to Withstand Space Radiation," *Crosslink*, Vol. 4, 203, pp. 30–35.

[16] McHale, J., "Space Avionics Systems Require Power Balanced Performance in Rad-Hard Processors," Tech. rep., Avionics Intelligence, 2009.

[17] Katz, D. and Some, R. R., "NASA Advances Robotic Space Exploration," *Computer*, Vol. 35, 2003, pp. 52–61.

[18] Levie, S., "Simple Mass Distribution for the Lunar Potential," Tech. rep., Bellcomm, Inc., 1971.

[19] Floberghagen, R., *Lunar Gravimetry Revealing the Far Side*, Kluwer Academic Publishers, Noordwijk, The Netherlands, 2002.

[20] Chatfield, A. B., *Fundamentals of High Accuracy Inertial Navigation*, Vol. 174 of *AIAA Progress in Astronautics and Aeronautics*, AIAA, Reston, Virginia, 1997.

[21] Ananda, M. P., "Farside Lunar Gravity from a Mass Point Model," *Proceedings of the 6th Lunar Science Conference*, March 1975.

[22] Ananda, M. P., "Mean Rates of the Orbital Elements of a Satellite Perturbed by a Lens-Shaped Mass Concentration," *Celestial Mechanics*, Vol. 12, 1975, pp. 495–511.

[23] Ananda, M. P., "Lunar Gravity a Mass Point Model," *Journal of Geophysical Research*, Vol. 82, No. 20, 1977, pp. 3049–3064.

[24] Wong, L., G. B., Downs, W., Sjogren, W., Muller, P., and Gottlieb., P., "A Surface-Layer Representation of the Lunar Gravitational Field," *Journal of Geophysical Research*, Vol. 76, No. 26, 1971, pp. 6220–6236.

[25] Levie, S., "Fitting a Mass Distribution to a Potential," Tech. rep., Bellcomm, Inc., 1971.

[26] Levie, S., "Potential Expansion for a Non-Homogeneous Oblate Spheriod," Tech. rep., Bellcomm, Inc., 1971.

[27] Lemoine, F. G., Luthcke, S. B., Rowlands, D. D., Chinn, D. S., Klosko, S. M., and Cox., C. M., "The Use of Mascons to Resolve Time-Variable Gravity from GRACE," *Dynamic Planet*, Vol. 130, 2005, pp. 231–234.

[28] Scott Luthcke, A. A., Rowlands, D., McCarthy, J., and Larsen, C., "Recent Glacier Mass Changes in the Gulf of Alaska Region from GRACE Mascon Solutions," *Journal of Glaciology*, Vol. 54, No. 188, 2008, pp. 767–777.

[29] Chao, B. F., "On Inversion for Mass Distribution from Global(Time-Variable) Gravity Field," *Journal of Geodynamics*, Vol. 39, 2005, pp. 223–230.

[30] Levie, S., "Transformation of Potential Function Under Coordinate Translations," Tech. rep., Bellcomm, Inc., 1970.

[31] Montenbruck, O. and Gill, E., *Satellite Orbits*, Springer, Berlin, Germany, 2000.

[32] Konopliv, A. S., Binder, A. B., Hood, L. L., Kucinskas, A. B., Sjogren, W. L., and Williams, J. G., "Improved Gravity Field of the Moon from Lunar Prospector," *Science*, Vol. 281, No. 5382, September 1998, pp. 1476–1480.

[33] Battin, R. H., *An Introduction to the Mathematics and Methods of Astrodynamics*, AIAA Education Series, AIAA, Reston, Virginia, 1999.

Appendices

Appendix A

Mass Estimation Scheme Derivation

Starting from equation

$$\int (v - \widetilde{v})^2 d\tau = \int (O^T S - O^T JM)^2 d\tau \tag{A.1}$$

Expanding the previous equation leads to

$$f(v, \widetilde{v}) = \int (v - \widetilde{v})^2 d\tau = (S - JM)^T W (S - JM) \tag{A.2}$$

Minimizing Equation A.2 by taking the derivative of $f(v, \widetilde{v})$ in respect to M results in

$$\frac{df}{dM} = \frac{d[(J^T M^T - S^T)W(S - JM)]}{dM} \tag{A.3}$$

Expanding out the Equation leads to

$$\frac{df}{dM} = \frac{d[(J^T M^T W S - J^T M^T W JM - S^T W S + S^T W JM)]}{dM} \tag{A.4}$$

Differentiating Equation A.4 results in

$$\frac{df}{dM} = (J^T W S - J^T W JM - J^T M^T W J + S^T W J) \tag{A.5}$$

After rearranging, Equation A.5 becomes

$$\frac{df}{dM} = 2J^T W S - 2J^T W JM \tag{A.6}$$

By setting

$$\frac{df}{dM} = 0 \tag{A.7}$$

in Equation A.6, and rearranging terms, results in the final equation

$$M = (J^T W J)^{-1} J^T W S \tag{A.8}$$

Appendix B

General Translation Transformation of Spherical Harmonic Coefficients

The the expansion coefficeints for an oblate or a prolate spheroid is

$$
\begin{bmatrix} C'_{km} \\ S'_{km} \end{bmatrix} = E_{k0}(2 - \sigma_{m0})\frac{(k-m)!}{(k+m)!}P_{km}(cos\theta)\begin{bmatrix} cos(m\vartheta) \\ sin(m\vartheta) \end{bmatrix} \tag{B.1}
$$

where E_{k0} is defined as

$$
E_{k0} = \sum_{L=0}^{k}(\frac{r'}{a})^{k-L}\frac{k!}{L!(k-L)!}C_{L0} \tag{B.2}
$$

The most general case can seen in Levie's research document, "Transformation of Potential Function Under Coordinate Translations" [30].

B.1 Point Mass Translation of Coefficients Derivation

From the mass configuration, the Stokes coefficients for the spherical harmonics can be computed in two ways:

$$
C_{nm} = \sum_{L=0}^{n}\frac{m_i}{m_{total}}C_{L0}(2 - \sigma_{m0})\frac{(n-m)!}{(n+m)!}\frac{n!}{L!(n-L)!}(\frac{R}{a})^{n-L}P_{nm}sin(\theta)cos(m\vartheta) \tag{B.3}
$$

and

$$
C_{nm} = \frac{2 - \sigma_{oj}}{M}\frac{(n-m)!}{(n+m)!}\iiint\left[\frac{R}{RE}\right]^{n}P_{nm}sin(\theta)cos(m\vartheta)p(r,\theta,\vartheta)r^2drd\theta d\vartheta \tag{B.4}
$$

Equation B.3 is a result of summing potentials of different masses. On the otherhand, Equation B.4 expresses the expansion coefficient with a mass distribution described by a density function.

To demonstrate that the previous equations are the same, the following is a proof for mass distribution of point masses. If Equation B.3 equals Equation B.4 then, there ratio should be equal to one. Taking the ratio of the previous two equations, and factoring out the common terms leads

to

$$\frac{C_{nm}}{C_{nm_2}} = \frac{\sum_{L=0}^{n} \frac{m_i}{m_{total}} C_{L0} \frac{n!}{L!(n-L)!} \left(\frac{R}{a}\right)^{n-L}}{\frac{1}{m_{total}} \int \int \int [\frac{R}{RE}]^n p(r,\theta,\vartheta) r^2 dr d\theta d\vartheta} \tag{B.5}$$

Since the density function is discrete when describing point masses, the integral can be taken as a sum. Hence, Equation B.5 becomes

$$\frac{C_{nm}}{C_{nm_2}} = \frac{\sum_{L=0}^{n} \frac{m_i}{m_{total}} C_{L0} \frac{n!}{L!(n-L)!} \left(\frac{R}{a}\right)^{n-L}}{[\frac{R}{RE}]^n \frac{1}{m_{total}} \sum_{i=1}^{w} \frac{m_i}{V} V} \tag{B.6}$$

Cancelling out equivalent terms leads to

$$\frac{C_{nm}}{C_{nm_2}} = \frac{\sum_{L=0}^{n} C_{L0} \frac{n!}{L!(n-L)!} \left(\frac{R}{a}\right)^{n-L}}{[\frac{R}{RE}]^n} \tag{B.7}$$

For point masses, the only non-zero expansion coefficient is C_{00}. So, the series in the numerator becomes

$$\frac{C_{nm}}{C_{nm_2}} = \frac{\left[\frac{R}{a}\right]^n}{[\frac{R}{RE}]^n} \tag{B.8}$$

However, the coefficient in the numerator is calibrated differently from the coefficient in the denominator. Recalibrating the coefficient in the numerator requires $\frac{a}{r} = \frac{a}{RE} \frac{RE}{r}$. Hence, Equation B.8 becomes

$$\frac{C_{nm}}{C_{nm_2}} = \frac{\left(\frac{R}{a}\right)^n [\frac{a}{RE}]^n}{[\frac{R}{RE}]^n} \tag{B.9}$$

Cancelling out similar terms in the previous equation leads to

$$\frac{C_{nm}}{C_{nm_2}} = \frac{[\frac{R}{RE}]^n}{[\frac{R}{RE}]^n} = 1 \tag{B.10}$$

Because the ratio is 1 between the two expressions for the stokes coefficients of mass points, then the equations are valid. To prove those equations are equivalent for more general cases requires a different, non-point mass, density function in Equation B.4, and a modification of Equation B.3.

The previous proof shows that the recalibration factor is correct. It also demonstrates that both Equations B.3 and B.4 generate the same spherical harmonic Stokes coefficients. In addition, the proof validates the formula for the translation of the Stokes coefficients by Sterling Levie.

Appendix C

Stokes Coefficients

C.1 LP 75D

Through lunar prospector and other satellites, fully normalized stokes coefficients in the spherical harmonic series were estimated for the moon. In Tables C.1, C.2, C.3, C.4, C.5, C.6, C.7 and C.8 are those stokes coefficients used in the thesis.

Table C.1: LP75D fully normalized stokes coefficients up to 10 degree 10 order. The equatorial radius is 1738 km, while the gravitational parameter is 4902.801056 $\frac{km^3}{s^2}$.

Degree	Order	Coefficients		Degree	Order	Coefficients	
n	m	C	S	n	m	C	S
0	0	1.00E+00	0.00E+00	7	5	-2.46E-07	1.10E-06
1	0	0.00E+00	0.00E+00	7	6	-1.02E-06	1.03E-06
1	1	0.00E+00	0.00E+00	7	7	-1.80E-06	-1.61E-06
2	0	-9.09E-05	0.00E+00	8	0	2.31E-06	0.00E+00
2	1	8.38E-09	7.71E-09	8	1	-4.21E-08	1.15E-06
2	2	3.46E-05	1.14E-08	8	2	3.06E-06	1.88E-06
3	0	-3.18E-06	0.00E+00	8	3	-1.85E-06	9.15E-07
3	1	2.63E-05	5.47E-06	8	4	3.37E-06	-4.90E-07
3	2	1.42E-05	4.88E-06	8	5	-1.17E-06	2.80E-06
3	3	1.23E-05	-1.77E-06	8	6	-1.62E-06	-2.21E-06
4	0	3.22E-06	0.00E+00	8	7	-1.55E-06	3.33E-06
4	1	-6.01E-06	1.63E-06	8	8	-2.50E-06	2.13E-06
4	2	-7.11E-06	-6.77E-06	9	0	-3.55E-06	0.00E+00
4	3	-1.37E-06	-1.34E-05	9	1	1.98E-06	2.78E-08
4	4	-6.03E-06	3.94E-06	9	2	2.01E-06	-1.50E-06
5	0	-2.22E-07	0.00E+00	9	3	-2.05E-06	2.29E-06
5	1	-1.03E-06	-4.09E-06	9	4	-1.96E-06	-1.37E-06
5	2	4.38E-06	1.12E-06	9	5	-1.54E-06	-3.64E-06
5	3	4.64E-07	8.68E-06	9	6	-2.23E-06	-2.86E-06
5	4	2.78E-06	3.20E-08	9	7	-3.89E-06	3.78E-08
5	5	3.12E-06	-2.76E-06	9	8	-1.27E-06	-2.26E-06
6	0	3.79E-06	0.00E+00	9	9	-9.51E-07	2.48E-06
6	1	1.52E-06	-2.58E-06	10	0	-1.00E-06	0.00E+00
6	2	-4.37E-06	-2.21E-06	10	1	8.40E-07	-9.69E-07
6	3	-3.27E-06	-3.51E-06	10	2	2.97E-07	-2.05E-07
6	4	3.58E-07	-4.05E-06	10	3	3.73E-07	8.11E-07
6	5	1.41E-06	-1.03E-05	10	4	-3.56E-06	1.49E-06
6	6	-4.71E-06	7.24E-06	10	5	7.78E-07	-3.28E-07
7	0	5.60E-06	0.00E+00	10	6	-4.07E-08	-1.93E-06
7	1	7.49E-06	-1.21E-07	10	7	-3.86E-06	-1.11E-06
7	2	-6.59E-07	2.42E-06	10	8	-3.70E-06	2.70E-06
7	3	6.04E-07	2.37E-06	10	9	-4.77E-06	-7.36E-09
7	4	-9.15E-07	8.57E-07	10	10	9.93E-07	-1.72E-06

Table C.2: LP75D fully normalized stokes coefficients from 11 degree 0 order to 15 order 11 degree. The equatorial radius is 1738 km, while the gravitational parameter is 4902.801056 $\frac{km^3}{s^2}$.

Degree	Order	Coefficients		Degree	Order	Coefficients	
n	m	C	S	n	m	C	S
11	0	-9.42E-07	0.00E+00	13	8	-2.78E-07	-1.57E-06
11	1	5.44E-09	6.01E-07	13	9	-8.15E-07	7.01E-07
11	2	7.43E-07	-2.01E-06	13	10	-6.16E-07	5.77E-07
11	3	3.58E-07	7.37E-07	13	11	-7.42E-07	3.09E-07
11	4	-9.77E-07	2.07E-06	13	12	-8.51E-07	-1.40E-06
11	5	1.54E-07	2.60E-06	13	13	2.35E-06	-2.70E-06
11	6	4.92E-07	-1.45E-06	14	0	4.52E-07	0.00E+00
11	7	-3.53E-07	-2.99E-06	14	1	6.42E-07	-6.18E-07
11	8	-2.26E-06	-1.51E-07	14	2	3.99E-07	2.83E-07
11	9	-2.04E-06	3.38E-07	14	3	7.08E-07	6.61E-10
11	10	-4.72E-06	-1.83E-07	14	4	-3.75E-07	-2.48E-06
11	11	-2.98E-06	-1.73E-06	14	5	-9.73E-07	-1.86E-07
12	0	-1.88E-06	0.00E+00	14	6	-6.43E-07	1.65E-06
12	1	-6.17E-07	1.54E-06	14	7	-6.61E-07	1.14E-06
12	2	-2.36E-07	1.59E-06	14	8	5.66E-08	8.82E-07
12	3	7.48E-07	-3.95E-06	14	9	2.25E-07	-1.16E-06
12	4	9.48E-07	-4.71E-07	14	10	-7.14E-08	1.87E-07
12	5	-7.47E-08	9.77E-07	14	11	-2.30E-06	2.00E-06
12	6	8.72E-07	6.54E-07	14	12	-2.05E-06	-4.22E-07
12	7	2.11E-06	-7.56E-07	14	13	5.86E-08	-1.20E-06
12	8	8.78E-07	-2.17E-06	14	14	-4.55E-07	1.18E-06
12	9	-1.22E-06	8.77E-07	15	0	-8.39E-08	0.00E+00
12	10	-3.53E-06	-1.24E-06	15	1	-9.67E-07	3.63E-07
12	11	-8.36E-07	-3.78E-07	15	2	-1.82E-07	7.82E-07
12	12	4.22E-07	1.24E-06	15	3	-1.21E-06	-6.75E-07
13	0	2.59E-07	0.00E+00	15	4	-1.07E-06	-1.26E-06
13	1	1.17E-06	-2.43E-08	15	5	-1.90E-07	-8.39E-07
13	2	-3.55E-06	5.79E-07	15	6	3.00E-08	-2.38E-07
13	3	-3.02E-07	-1.61E-06	15	7	1.35E-06	1.65E-06
13	4	9.55E-07	-6.94E-07	15	8	1.67E-06	2.02E-06
13	5	-1.29E-06	1.23E-06	15	9	6.61E-08	-1.63E-06
13	6	3.35E-08	1.34E-06	15	10	-5.00E-07	-9.44E-08
13	7	1.15E-07	-9.38E-07	15	11	-2.06E-06	-9.52E-07

Table C.3: LP75D fully normalized stokes coefficients from 15 degree 12 order to 19 order 7 degree. The equatorial radius is 1738 km, while the gravitational parameter is 4902.801056 $\frac{km^3}{s^2}$.

Degree	Order	Coefficients		Degree	Order	Coefficients	
n	m	C	S	n	m	C	S
15	12	-1.05E-06	-7.95E-07	17	12	2.02E-08	-4.33E-08
15	13	1.62E-07	3.88E-07	17	13	-2.10E-07	-5.94E-08
15	14	4.25E-07	7.86E-07	17	14	1.35E-06	-5.05E-07
15	15	3.72E-07	5.68E-07	17	15	4.01E-07	3.78E-07
16	0	3.60E-07	0.00E+00	17	16	-4.96E-07	-1.35E-07
16	1	-8.15E-08	9.56E-07	17	17	-6.20E-07	1.17E-06
16	2	1.75E-06	-1.12E-07	18	0	-5.75E-07	0.00E+00
16	3	1.11E-08	3.61E-07	18	1	2.10E-07	-6.45E-08
16	4	4.41E-07	4.83E-07	18	2	-2.21E-07	-5.97E-07
16	5	7.80E-07	-6.31E-07	18	3	8.48E-07	6.01E-07
16	6	1.05E-06	-9.52E-07	18	4	-8.54E-07	1.02E-06
16	7	-2.25E-07	-7.90E-07	18	5	-2.28E-07	9.34E-08
16	8	-3.52E-07	2.22E-07	18	6	-1.67E-06	8.41E-07
16	9	-1.39E-06	-1.11E-06	18	7	-1.50E-07	-1.04E-06
16	10	2.32E-07	7.95E-07	18	8	6.25E-07	-9.57E-08
16	11	4.24E-07	1.21E-06	18	9	6.50E-07	-1.04E-06
16	12	-8.59E-07	4.28E-07	18	10	-4.12E-08	-6.20E-07
16	13	-1.12E-06	4.36E-07	18	11	-3.63E-07	-1.83E-06
16	14	-1.18E-06	-2.71E-07	18	12	1.20E-06	9.56E-07
16	15	-4.63E-08	-1.22E-06	18	13	-3.26E-07	-2.03E-07
16	16	-7.04E-07	-6.22E-07	18	14	-8.62E-09	-7.71E-07
17	0	-1.06E-06	0.00E+00	18	15	-4.80E-07	-2.16E-07
17	1	6.94E-07	-4.45E-08	18	16	4.02E-07	-1.43E-06
17	2	-1.25E-07	-1.13E-06	18	17	1.29E-06	-4.35E-07
17	3	-2.07E-07	-3.40E-07	18	18	7.70E-08	3.72E-08
17	4	9.92E-07	2.17E-06	19	0	2.48E-10	0.00E+00
17	5	3.55E-07	-8.09E-07	19	1	-2.65E-07	1.51E-07
17	6	7.59E-07	-1.30E-06	19	2	3.99E-07	-4.26E-07
17	7	-1.61E-06	-1.22E-06	19	3	-9.84E-07	9.81E-07
17	8	-3.63E-07	-1.63E-07	19	4	-9.17E-07	-1.04E-06
17	9	7.58E-07	1.44E-06	19	5	1.55E-09	1.36E-06
17	10	1.21E-06	1.05E-06	19	6	2.23E-08	2.32E-07
17	11	9.59E-07	-1.01E-06	19	7	1.00E-06	5.13E-07

Table C.4: LP75D fully normalized stokes coefficients from 19 degree 8 order to 22 order 10 degree. The equatorial radius is 1738 km, while the gravitational parameter is 4902.801056 $\frac{km^3}{s^2}$.

Degree	Order	Coefficients		Degree	Order	Coefficients	
n	m	C	S	n	m	C	S
19	8	3.11E-07	6.72E-07	21	0	-8.98E-08	0.00E+00
19	9	-8.68E-08	-1.15E-08	21	1	-3.11E-08	6.39E-07
19	10	-6.95E-07	2.64E-07	21	2	-1.52E-06	-7.20E-08
19	11	3.35E-07	-1.02E-07	21	3	5.07E-07	-1.14E-06
19	12	4.67E-07	2.57E-07	21	4	-4.05E-07	6.22E-07
19	13	2.28E-07	1.73E-06	21	5	1.25E-07	2.05E-07
19	14	-7.56E-07	9.76E-07	21	6	-2.19E-07	-3.72E-07
19	15	2.81E-07	-8.23E-07	21	7	-2.03E-07	4.16E-07
19	16	3.69E-07	-3.11E-08	21	8	-6.04E-07	-2.50E-07
19	17	-4.64E-07	-5.51E-07	21	9	-1.62E-07	-4.90E-07
19	18	1.10E-06	-2.42E-07	21	10	-3.50E-07	-5.05E-07
19	19	2.80E-07	9.67E-08	21	11	-2.39E-07	2.95E-07
20	0	5.65E-07	0.00E+00	21	12	9.45E-08	9.13E-07
20	1	5.13E-08	-5.80E-07	21	13	-1.40E-07	-1.04E-07
20	2	4.47E-07	1.06E-07	21	14	-1.47E-07	7.10E-07
20	3	3.46E-07	-6.70E-08	21	15	-8.61E-07	2.21E-07
20	4	8.49E-07	-6.42E-07	21	16	1.09E-06	3.92E-07
20	5	2.91E-07	-3.83E-07	21	17	9.05E-07	2.18E-07
20	6	-4.89E-07	5.59E-07	21	18	1.18E-07	-5.44E-07
20	7	-7.63E-07	-5.31E-07	21	19	2.71E-06	9.60E-07
20	8	5.30E-07	-1.17E-08	21	20	-5.66E-07	2.08E-06
20	9	2.68E-07	4.45E-07	21	21	-6.22E-07	1.28E-07
20	10	2.55E-07	-3.88E-07	22	0	9.05E-08	0.00E+00
20	11	-5.28E-08	5.92E-07	22	1	-4.25E-08	3.90E-07
20	12	-1.09E-07	-1.05E-06	22	2	-6.28E-07	-2.19E-07
20	13	5.58E-07	1.46E-07	22	3	7.12E-07	4.71E-07
20	14	4.14E-07	3.01E-07	22	4	5.25E-07	1.84E-07
20	15	-2.97E-08	-5.68E-07	22	5	1.43E-07	-8.55E-07
20	16	7.56E-07	6.41E-07	22	6	-2.56E-07	2.34E-07
20	17	5.71E-07	-8.05E-07	22	7	4.15E-07	6.54E-07
20	18	1.00E-07	-1.18E-06	22	8	2.02E-07	-3.21E-07
20	19	-1.49E-07	6.88E-07	22	9	6.08E-07	3.89E-07
20	20	1.94E-07	-1.44E-07	22	10	-3.10E-07	6.25E-07

Table C.5: LP75D fully normalized stokes coefficients from 22 degree 11 order to 25 order 4 degree. The equatorial radius is 1738 km, while the gravitational parameter is 4902.801056 $\frac{km^3}{s^2}$.

Degree	Order	Coefficients		Degree	Order	Coefficients	
n	m	C	S	n	m	C	S
22	11	4.16E-07	-2.32E-07	23	21	3.77E-08	6.25E-07
22	12	-3.60E-08	-4.41E-07	23	22	-1.04E-06	-7.65E-07
22	13	-6.40E-07	-1.97E-07	23	23	-1.15E-06	2.90E-08
22	14	-9.07E-07	1.09E-06	24	0	-1.54E-07	0.00E+00
22	15	-8.84E-08	-4.34E-07	24	1	7.56E-08	-1.23E-07
22	16	-2.99E-07	3.16E-07	24	2	7.24E-07	2.19E-07
22	17	-7.48E-07	-5.76E-07	24	3	2.14E-07	-1.15E-06
22	18	6.33E-07	6.35E-07	24	4	7.38E-08	2.77E-07
22	19	-9.12E-07	-1.34E-07	24	5	-1.08E-07	-3.64E-08
22	20	-1.43E-07	-9.99E-07	24	6	-9.90E-08	-8.38E-08
22	21	-2.84E-08	5.02E-07	24	7	4.28E-07	2.57E-08
22	22	5.57E-07	8.64E-07	24	8	4.32E-07	4.16E-07
23	0	-8.59E-08	0.00E+00	24	9	-1.09E-06	-2.65E-07
23	1	-1.14E-07	-8.24E-07	24	10	-2.43E-07	8.56E-08
23	2	1.67E-07	-5.69E-08	24	11	4.80E-07	4.80E-08
23	3	-2.21E-07	3.48E-07	24	12	1.14E-06	8.10E-08
23	4	4.02E-07	-6.29E-07	24	13	6.65E-07	-7.31E-08
23	5	-5.65E-07	7.92E-07	24	14	7.89E-07	-1.04E-06
23	6	5.48E-07	2.87E-07	24	15	-4.57E-08	3.04E-07
23	7	5.64E-07	-9.67E-07	24	16	5.76E-07	-3.39E-07
23	8	5.74E-07	-2.63E-07	24	17	7.13E-07	1.03E-07
23	9	8.38E-07	8.60E-08	24	18	-9.22E-07	-7.25E-07
23	10	-7.93E-07	-1.86E-07	24	19	6.16E-07	-5.02E-07
23	11	7.36E-08	7.38E-08	24	20	-2.36E-07	-3.13E-07
23	12	-2.53E-07	-8.89E-07	24	21	-4.05E-07	-4.89E-07
23	13	-7.68E-07	6.80E-07	24	22	-2.15E-07	3.75E-07
23	14	8.35E-07	-2.01E-07	24	23	-1.01E-07	-2.88E-07
23	15	8.42E-08	1.89E-07	24	24	9.74E-07	-7.53E-07
23	16	-7.18E-07	4.49E-07	25	0	-1.46E-07	0.00E+00
23	17	-4.84E-07	-2.20E-07	25	1	-1.24E-07	3.81E-07
23	18	-6.44E-08	4.90E-07	25	2	-5.39E-07	-2.80E-07
23	19	-1.82E-07	-4.23E-07	25	3	6.47E-07	7.76E-08
23	20	6.05E-07	1.06E-06	25	4	-9.53E-07	2.39E-08

Table C.6: LP75D fully normalized stokes coefficients from 25 degree 5 order to 27 order 17 degree. The equatorial radius is 1738 km, while the gravitational parameter is 4902.801056 $\frac{km^3}{s^2}$.

Degree	Order	Coefficients		Degree	Order	Coefficients	
n	m	C	S	n	m	C	S
25	5	4.23E-07	7.61E-07	26	12	-5.10E-07	-8.07E-07
25	6	2.54E-10	3.94E-07	26	13	2.47E-07	7.66E-07
25	7	6.20E-07	9.63E-07	26	14	-2.93E-08	2.18E-07
25	8	-1.14E-06	1.03E-06	26	15	1.66E-07	-7.74E-08
25	9	-3.98E-07	-1.85E-08	26	16	-9.63E-08	1.27E-07
25	10	5.37E-07	9.49E-07	26	17	-6.44E-08	1.09E-07
25	11	-9.81E-08	-3.59E-07	26	18	2.46E-07	3.27E-07
25	12	-1.56E-07	-4.21E-07	26	19	1.11E-08	3.65E-08
25	13	3.09E-07	1.44E-07	26	20	-1.01E-07	8.45E-07
25	14	-8.16E-07	4.65E-07	26	21	-2.99E-07	-1.42E-07
25	15	1.87E-07	3.69E-07	26	22	-1.11E-06	4.32E-07
25	16	-4.19E-08	-6.10E-07	26	23	-1.84E-07	-1.65E-07
25	17	-3.02E-07	-4.08E-07	26	24	-5.46E-07	-5.39E-07
25	18	-2.30E-07	2.76E-07	26	25	-1.33E-07	-2.49E-07
25	19	-9.16E-07	-1.86E-07	26	26	8.22E-08	4.52E-07
25	20	-2.76E-07	-7.39E-07	27	0	-9.40E-07	0.00E+00
25	21	7.21E-07	1.36E-07	27	1	8.68E-07	5.25E-08
25	22	2.33E-07	-3.71E-07	27	2	7.98E-08	-4.22E-07
25	23	9.58E-07	1.10E-07	27	3	1.24E-07	-7.09E-10
25	24	1.11E-06	8.65E-08	27	4	-4.18E-07	3.90E-07
25	25	-9.11E-08	4.60E-07	27	5	-3.40E-07	2.11E-08
26	0	-1.71E-07	0.00E+00	27	6	-1.55E-07	3.34E-07
26	1	-1.47E-07	8.25E-08	27	7	2.31E-07	-1.66E-07
26	2	9.87E-07	3.63E-09	27	8	-6.53E-08	-8.64E-08
26	3	1.28E-07	8.44E-07	27	9	-4.39E-07	-1.49E-07
26	4	9.40E-08	8.94E-08	27	10	2.81E-07	-5.20E-07
26	5	4.04E-07	-6.66E-07	27	11	7.67E-08	-4.02E-07
26	6	-5.29E-07	-2.45E-07	27	12	-2.70E-07	-4.74E-07
26	7	-1.31E-07	-5.37E-07	27	13	4.27E-07	-1.54E-07
26	8	-1.18E-07	3.14E-07	27	14	5.50E-07	-9.46E-07
26	9	6.70E-08	6.56E-07	27	15	-4.79E-08	2.68E-07
26	10	-1.10E-07	1.16E-08	27	16	5.79E-08	2.23E-07
26	11	-2.49E-07	1.59E-07	27	17	7.07E-08	8.89E-07

Table C.7: LP75D fully normalized stokes coefficients from 27 degree 18 order to 29 order 26 degree. The equatorial radius is 1738 km, while the gravitational parameter is 4902.801056 $\frac{km^3}{s^2}$.

Degree	Order	Coefficients		Degree	Order	Coefficients	
n	m	C	S	n	m	C	S
27	18	-8.39E-08	-6.79E-07	28	23	8.91E-08	4.01E-07
27	19	-2.40E-08	-3.51E-07	28	24	2.04E-07	8.85E-08
27	20	1.27E-07	-2.80E-07	28	25	6.91E-07	-2.35E-07
27	21	2.86E-07	-6.86E-07	28	26	3.09E-07	7.45E-07
27	22	6.18E-07	5.59E-07	28	27	-1.91E-07	5.73E-07
27	23	1.71E-07	-4.33E-07	28	28	1.90E-07	-1.64E-07
27	24	7.49E-07	-3.23E-07	29	0	-6.52E-07	0.00E+00
27	25	-6.15E-07	9.97E-07	29	1	1.20E-07	-3.22E-07
27	26	-3.16E-07	-5.20E-07	29	2	-2.20E-07	-3.80E-07
27	27	-4.40E-07	-1.46E-07	29	3	-2.71E-07	5.67E-08
28	0	7.81E-07	0.00E+00	29	4	-1.03E-08	-2.71E-09
28	1	2.75E-07	6.24E-07	29	5	1.08E-07	2.62E-08
28	2	-1.56E-07	8.33E-07	29	6	-3.91E-07	-2.42E-07
28	3	-5.49E-07	1.05E-07	29	7	-8.11E-08	-3.05E-07
28	4	-5.72E-07	3.51E-08	29	8	5.54E-07	-5.95E-08
28	5	3.22E-07	-2.91E-08	29	9	2.50E-07	-5.94E-07
28	6	2.52E-07	5.47E-08	29	10	3.57E-07	2.32E-07
28	7	-4.27E-07	2.21E-07	29	11	-5.99E-08	1.67E-07
28	8	-2.12E-07	-1.15E-07	29	12	-3.45E-07	-4.43E-07
28	9	-1.46E-07	3.66E-08	29	13	3.02E-07	4.18E-07
28	10	-4.78E-07	-6.34E-07	29	14	-7.83E-09	7.89E-07
28	11	-1.71E-07	-1.75E-07	29	15	-7.58E-08	8.26E-08
28	12	3.20E-07	-1.01E-07	29	16	3.96E-07	-1.80E-07
28	13	4.02E-07	-3.20E-07	29	17	-3.84E-07	-4.66E-07
28	14	1.68E-07	-2.90E-07	29	18	-5.29E-08	-1.42E-07
28	15	-6.32E-07	4.63E-07	29	19	-3.22E-07	-7.20E-08
28	16	-1.79E-07	-6.85E-07	29	20	-3.77E-07	3.07E-07
28	17	-5.62E-08	-2.66E-08	29	21	1.46E-08	-6.31E-08
28	18	1.61E-07	5.26E-07	29	22	-5.14E-07	-1.29E-07
28	19	1.55E-07	-3.11E-08	29	23	3.50E-07	1.21E-07
28	20	2.90E-07	-2.91E-07	29	24	1.54E-09	5.60E-08
28	21	3.24E-08	-2.45E-07	29	25	2.13E-09	-7.82E-08
28	22	-5.93E-07	1.49E-07	29	26	1.22E-08	-6.40E-07

Table C.8: LP75D fully normalized stokes coefficients from 29 degree 7 order to 30 order 30 degree. The equatorial radius is 1738 km, while the gravitational parameter is 4902.801056 $\frac{km^3}{s^2}$.

Degree	Order	Coefficients	
n	m	C	S
29	27	1.50E-07	7.94E-08
29	28	-1.33E-07	2.17E-07
29	29	1.29E-07	-4.68E-08
30	0	3.25E-07	0.00E+00
30	1	-1.94E-09	1.80E-07
30	2	-5.52E-07	-4.01E-07
30	3	-3.78E-07	1.52E-07
30	4	1.71E-07	-8.38E-08
30	5	-7.93E-08	-3.12E-07
30	6	-1.15E-08	4.24E-07
30	7	-1.49E-07	-2.21E-07
30	8	-3.27E-07	-5.22E-07
30	9	-2.46E-07	-4.97E-08
30	10	-3.41E-07	-8.58E-08
30	11	6.87E-08	-2.38E-07
30	12	-1.74E-07	5.04E-07
30	13	-1.01E-08	4.80E-07
30	14	4.14E-07	-1.93E-07
30	15	-4.12E-07	9.56E-08
30	16	1.86E-07	-2.90E-07
30	17	3.51E-07	4.57E-07
30	18	2.10E-07	1.55E-07
30	19	-3.00E-07	1.49E-07
30	20	1.80E-07	8.37E-08
30	21	1.28E-07	1.62E-07
30	22	1.80E-07	7.78E-07
30	23	-1.93E-07	-1.17E-07
30	24	-2.49E-07	1.81E-07
30	25	9.04E-08	9.16E-08
30	26	-7.30E-08	8.79E-09
30	27	6.13E-08	4.41E-07
30	28	-1.67E-07	-3.60E-07
30	29	1.61E-07	-1.45E-08
30	30	-3.11E-07	9.74E-07